



## Article

# Effects of Vegetation Belt Movement on Wildfire in the Mongolian Plateau over the Past 40 Years

Lumen Chao <sup>1,2</sup>, Yulong Bao <sup>1,3,\*</sup>, Jiquan Zhang <sup>4,5</sup> , Yuhai Bao <sup>1,3</sup>, Li Mei <sup>1</sup> and Ersi Cha <sup>1</sup><sup>1</sup> College of Geographic Science, Inner Mongolia Normal University, Hohhot 010022, China<sup>2</sup> College of Resources and Environment, Baotou Teachers' College, Science and Technology University of Inner Mongolia, Baotou 014030, China<sup>3</sup> Inner Mongolia Key Laboratory of Remote Sensing and Geographic Information Systems, Inner Mongolia Normal University, Hohhot 010022, China<sup>4</sup> School of Environment, Northeast Normal University, Changchun 130024, China<sup>5</sup> Key Laboratory for Vegetation Ecology, Ministry of Education, Changchun 130024, China

\* Correspondence: baoyulong@imnu.edu.cn; Tel.: +86-153-2600-2297

**Abstract:** The frequency and intensity of fires are increasing because of warmer temperatures and increased droughts, as well as climate-change induced fuel distribution changes. Vegetation in environments, such as those in the mid-to-high latitudes and high elevations, moves to higher latitudes or elevations in response to global warming. Over the past 40 years, the Mongolian Plateau has been arid and semi-arid, with a decrease in growing season vegetation in the southwest and an increase in growing season vegetation in the northeast. The northward movement of vegetation has brought fires, especially in the Dornod, Sukhbaatar, and Kent provinces near the Kent Mountains, and has become more obvious in the past 20 years. The occurrence of a dead fuel index (DFI) with high probability is distributed in northern Mongolia, the border area between China and Mongolia, and the forest-side meadow-steppe region of the Greater Khingan Mountains. These findings suggest that vegetation is moving northward because of climate change and this presents a challenge of future warming spreading fire northward, adding material to the study of the relationship between the northward movement of global vegetation and fires.

**Keywords:** fuel; wildfire; vegetation movement; Mongolian Plateau



**Citation:** Chao, L.; Bao, Y.; Zhang, J.; Bao, Y.; Mei, L.; Cha, E. Effects of Vegetation Belt Movement on Wildfire in the Mongolian Plateau over the Past 40 Years. *Remote Sens.* **2023**, *15*, 2341. <https://doi.org/10.3390/rs15092341>

Academic Editor: William W. Hargrove

Received: 10 March 2023

Revised: 22 April 2023

Accepted: 25 April 2023

Published: 28 April 2023



**Copyright:** © 2023 by the authors. Licensee MDPI, Basel, Switzerland. This article is an open access article distributed under the terms and conditions of the Creative Commons Attribution (CC BY) license (<https://creativecommons.org/licenses/by/4.0/>).

## 1. Introduction

Climate change influences the distribution of species and ecosystems [1,2]. Many studies have found that vegetation and trees in high latitudes and high elevations are moving upwards or downwards, owing to the rapid increase in temperature caused by climate change [3]. Harsch et al. analyzed tree line dynamics at 166 locations worldwide and found that tree lines advanced more than 52% forward, while only 1% declined [4]. Mekonnen et al. calculated shrub expansion in the Arctic tundra and concluded that climate change has led to high-latitude tundra shrubification [5]. In addition, upward (higher elevation), northward (higher latitude), and westward shifts of plants have been found in mid-latitude mountainous regions [6,7]. Kelly et al. found that the predominant plants in Southern California in 1977 and in 2006–2007 increased by 65 m of plant cover along a gradient of 2314 m above sea level [6]. As the timescale was extended and the study area expanded, Crimmins et al. observed that the slope of plant species in California decreased in 1930–2005 [7]. Using 151 species of in the Hengduan Mountains Region and modeling their distribution from the last glacial period to 2050, Liang et al. concluded that, due to uneven terrain along the elevation gradient, plants are moving northward, toward the west, and in other directions. Previous studies have demonstrated that global warming affects vegetation distribution in cold environments, such as the North Pole and mid-latitude mountains [8]. Under climate change, movement of vegetation belts appeared

at mid-high-latitude and higher elevations. Combustibles (mainly vegetation) are key factors in fire development [9,10] and carbon emissions because they determine where fires are likely to occur, and the amount of carbon released. With global warming, the diffusion and accumulation of vegetation may cause more fires, particularly when the risk of lightning (the main source of fire) increases [11]. Therefore, the northward movement of vegetation is closely related to fires [12].

There are three essential elements for a fire to occur: combustibles (vegetation in its natural state), meteorological elements, and fire sources. Combustibles are the most basic and complex elements. The combustible material used in this study was natural vegetation. Combustibles are dangerous in environments that experience frequent disasters, such as grassland fires. Environments that experience frequent disasters are key determining factors in the occurrence and spread of grassland fires. Terrain, fuel, and weather are the three factors that can create and sustain a fire, with fuel being the most complex and important factor that drives fire behavior [13,14]. Grassland fire behavior refers to the characteristics of the fire spread and development process after ignition, that is, the fire process characteristics from ignition to development until the weakening and extinction of the flames [15]. The amount of fuel on the ground and the continuity of vegetation influences the spread and reach of fire [16–18]. The fuel influences the fire in many ways, for example, spreading speed, fire behavior et al.

Meanwhile, wildfire predictions and risk assessments are necessary. These wildfire models use remote sensing and precise spatial combustible data, and can afford high resolution spatial data for the region [19]. Temperature and burning area are positively correlated depending on the vegetation available for burning [20]. Simulated fire models can obtain the processes that control surface fuel' finish time, and these models depend on combustibles to lead fire behavior and spread [21]. Using combustible coverage and height, the Mallee heath fire spread model derives the shape, unburned area, and extent of the fire area within the fire range [19]. The extent to which the vegetation surface is burned by fire each year is influenced by several factors, including climate, fuel available type and human impacts. Before hominids evolved, the burn area was determined by the climate, which directly affected vegetation, drought, and lightning [22]. The role of current and future fuel restrictions on a regional scale remains unclear. Fuel availability is the feedback of understudied wildfire trends on a regional scale and only modestly reduces the predictions of climate- driven trends in fire areas [23]. In climate fire model predictions, fuel availability has a certain effect on the fire region, which increased by 46% to 90% from the 1991–2020 baseline to the 2020–2050 baseline under different intensities of fuel fire feedback, compared to 107% in the constant fuel case [24]. Remote sensing and models have played an important role of in wildfire fuel research. *Eucalyptus globulus* has an increased chance of survival in future climate scenarios in the northern hemisphere, particularly in mid-latitudes, verifying a northward expansion of vegetation under climate change response [25]. Greater burning of the Arctic tundra would accelerate the northward migrating of the boreal trees, potentially accelerating the positive feedback related to permafrost carbon release [11]. Fires threaten the security of ecosystems and release lots of carbon into the air through vegetation burning [26]. The intensity and frequency of fires have risen owing to droughts and higher temperatures over the past several decades [25,27]. However, little research has been conducted on the effects of vegetation movement on fires in the vulnerable area of the Mongolian Plateau. It is well known that vegetation movement is directly related to future fire distribution, as the spread over vegetation confirms where fires are likely to occur [28–30]. Combined with the increases in temperature and human ignition [31,32], ecosystems in the northern hemisphere will be challenged by more fires in the future. To better manage fires and reduce carbon emissions, focus must be on the dynamics of fire and vegetation development. The relationship growth between fuel dryness and fire region and future tendency in fire areas and extreme fire years increased in all cases [23]. The fire and fuel relationship of the Mongolian Plateau is important in the northern hemisphere ecosystem.

Fires are particularly prominent in the densely populated temperate flammable forests and sparsely populated flammable northern regions of Mongolia, leading to greenhouse gas emissions [10]. In the Mongolian Plateau, under climate change, the vegetation changes more obviously in the natural state [33,34], and the Mongolian Plateau also has more occurrences of fires [35–38]; fires are more frequent in dead combustible areas with high flammability and are higher risk. Carbon emissions from fires also increase with climate change [39,40]. Additionally, vegetation belt changes are obvious in the Mongolian Plateau in the arid and semi-arid regions [41]. The fire and increased carbon emissions were caused by dead combustibles.

Under climate change over the past 40 years, changes in vegetation belts have become obvious globally. With these changes, the vegetation withering period will also move northward [42], thereby affecting the vegetation and coverage of withered grass, which in turn affects the occurrence area of fires and the probability of fire occurrence. However, some researches have concentrated on the relationships among vegetation movement, distribution, and fire occurrence. The objective of this study is to determine the change and movement of the vegetation belt with climate change over the past 40 years and its influence on fire occurrence. Accurate estimation of vegetation dynamics, particularly the relationship between fire occurrence and the movement of vegetation belts, is critical for effective fire management and carbon emission reduction. To facilitate wildfire monitoring and prevention, especially as global warming leads to increasing fires, it is necessary to understand the distribution and changes in fire-prone vegetation in a changing climate with better management and control policies. The study area has a high probability of fire occurrence, regardless of fire management and human activities.

The objectives of this research are to: (1) study the change and movement of vegetation belts on the Mongolian Plateau over the past 40 years, (2) study the relationship between the movement of vegetation belts in the Mongolian Plateau and fires, and (3) study the relationship between DFI and fires in Mongolian Plateau grasslands. This study investigates the northward migration of vegetation due to climate change, and the challenge of expanding fire northward in future warming and adds to the study on the relationship between northward global vegetation movement and fire.

## 2. Materials and Methods

### 2.1. Study Area

The Mongolian Plateau (Inner Mongolia Autonomous Region of China and Mongolia) is a unique arid and semi-arid region, and various economic activities affect its ecosystem [43–46]. Under global climate change, the natural ecological environment is fragile and sensitive [47]. Among the grassland ecosystems worldwide it is one of the largest, upping to 2.76 million square kilometers areas, with unique natural and climate characteristics [48]. The Inner Mongolia Autonomous Region accounts for 68% of the total length of the China-Mongolia border, with a length of 3193 km [35]. The long-term changes in biomass in the Mongolian Plateau indicate great geographic differences, with non-significant changes in vegetation, which accounted for 35% in Inner Mongolia and 44% in Mongolia [49,50]. The Mongolian Plateau is located from the Gobi Desert in Central Asia to the Siberian taiga forest [51,52]. There is a typical continental climate characteristic with hot summers and cold winters. Under the influence of climate differentiation, the vegetation showed obvious horizontal and vertical zonation. Many vegetation types in arid and semi-arid regions, such as forests, meadows, shrubs, typical desert steppes, Gobi vegetation, and grasslands, account for approximately 70% of the plateau [34,53]. The study area comprises the Mongolian Plateau (a), elevation (b), vegetation type (c), and the same-level administrative divisions in League (City) (d) (Figure 1). With a population of 2.2 per square kilometer, Mongolia is a country with a low population density, and because of long-term nomadism, humans have less impact on the ecosystem (<http://1212.mn/2021> accessed on 9 September 2022).

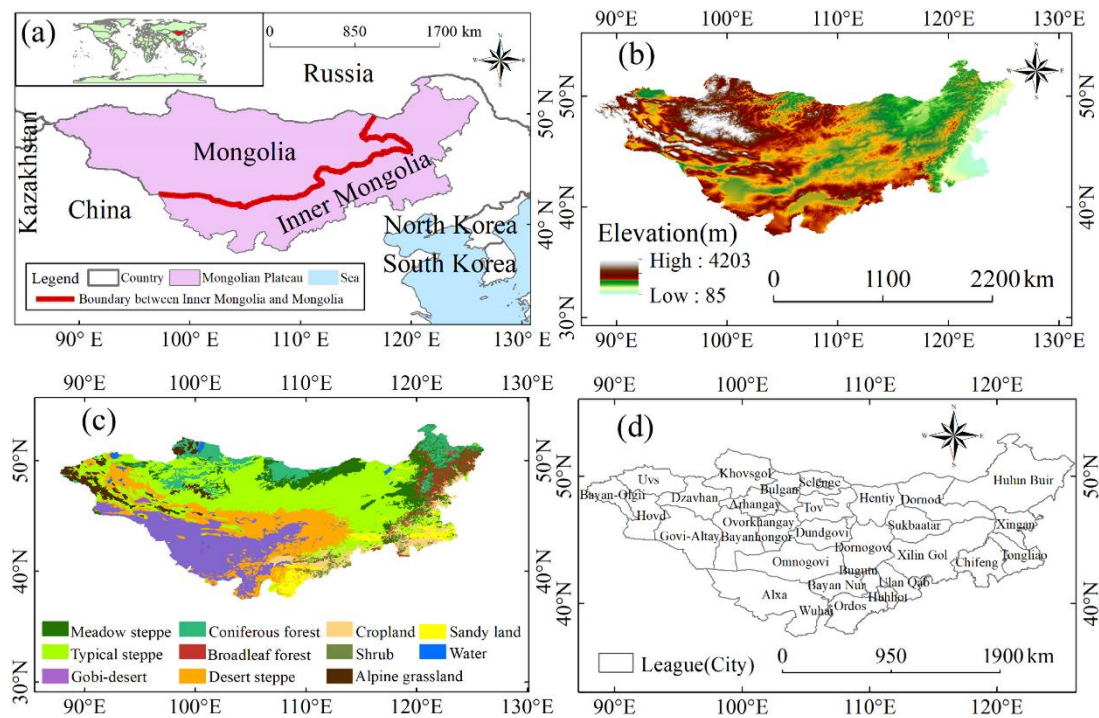


**Figure 1.** (a) Location of study area; (b) elevation; (c) grassland types of study area; (d) League (City).

## 2.2. Data

Our study employed both the Advanced Very High-Resolution Radiometer (AVHRR) Global Inventory Monitoring and Modelling Studies (GIMMS) NDVI and Moderate-Resolution Imaging Spectroradiometer (MODIS) NDVI products. Specifically, AVHRR GIMMS NDVI data (<https://ecocast.arc.nasa.gov/> (accessed on 23 December 2022)), with a temporal resolution of 15-days and spatial resolution of 8 km, from 1982 to 2015, and MOD13A2 NDVI, which had a spatial resolution of 500 m and 16-day intervals from 2001 to 2020. NDVI is typically used to detect vegetation [31,38]. GIMMS NDVI was used to analyze vegetation coverage, desertification, and phenology [41]. The NDVI data were analyzed with a minimum temporal resolution of months, so it was necessary to synthesize the monthly GIMMS NDVI values with a 15-day temporal resolution. In this study, the monthly maximum value composite (MVC) method was used to synthesize the AVHRR GIMMS NDVI and MODIS NDVI data; that is, the maximum value of the two 15-day NDVI datasets of a month were selected as the NDVI value for the month. The time resolution of MODIS NDVI is 16 days; therefore, monthly data synthesis was also required, using a method consistent with GIMMS AVHRR NDVI [54]. The NDVI values were calculated from April to October averaged to obtain the mean NDVI, and it is belonged to the growing season. Python3.6 was used for data processing.

Precipitation and temperature that were used in this paper were obtained from the fifth generation of the European Center for Medium-Range Weather Forecasts Interim Re-Analysis (ERA5) (<https://cds.climate.copernicus.eu/> (accessed on 23 December 2022)). ERA5 is a spatial resolution of  $0.25^{\circ} \times 0.25^{\circ}$  and provides the hourly data of many atmospheric, terrestrial, and oceanic climate variables. In this paper, we used the ERA5 data of the monthly mean air temperature 2 m above the surface and precipitation data from 1982 to 2020. The vegetation data of spatial resolution were  $0.083^{\circ}$  (8 km), and the ERA5 data were resampled by the ArcGIS10.5 software.

MOD09A1 16-Day L3 Global 1 km SIN Grid data from 2000 to 2020 were used to calculate DFI, and MCD64A1 had a spatial resolution of 500 m and 16-day intervals from 2001–2020 for burned area data.

### 2.3. Method

#### 2.3.1. Integration and Validation with AVHRR GIMMS and MODIS NDVI Data

To implement the use of data time series length, the two NDVI datasets were integrated using a corresponding pixel linear regression model. The two datasets overlap from 2001 to 2015. The linear regression model was established from the two NDVI products from 2001–2010, and the remaining datasets from 2011–2015 were used for cross-validation. To avoid mismatches between these two datasets, the MODIS NDVI datasets at 500 m × 500 m were resampled to an 8 km × 8 km resolution. The detailed regression model formula is as follows [42]:

$$G_i = aM_i + b + \sigma_i \quad (1)$$

$$a = \frac{\sum_{i=1}^n (G_i - \bar{M})(G_i - \bar{G})}{\sum_{i=1}^n (M_i - \bar{M})^2} \quad (2)$$

$$b = \bar{G} - a\bar{M} \quad (3)$$

where  $G_i$  and  $M_i$  represent the AVHRR and MODIS NDVI (8 km × 8 km) in the  $i_{th}$  month;  $\sigma_i$  is the error value;  $G$  and  $M$  are the mean values of  $G_i$  and  $M_i$  from 2001–2009, respectively;  $n$  is the regression model of the number years ( $n$  is equal with 10 in this paper); and  $a$  and  $b$  are the regression model slope and intercept, respectively, 1.03 and 0.0037.

Cross-validation was used to assess the regression model quality. Regression coefficients ( $a$  and  $b$ ) were used to calculate the MODIS NDVI data from 2010–2015 to get the extended GIMMS NDVI data, and they were evaluated using the extended GIMMS NDVI and raw GIMMS NDVI data. Raw GIMMS NDVI and extended GIMMS NDVI data from 2010 to 2015, for which the  $R$  of value was 0.95, demonstrated the application of the integrated method in the study area. The GIMMS NDVI can be extended to apply to the new regression model from the MODIS NDVI from 2016–2020. The long-term series lengthened GIMMS NDVI from 1982 to 2020 and was applied to calculate this study's NDVI.

#### 2.3.2. Emerging Hot Spot Analysis

Emerging hot spot analysis (EHSA) is analysis to explore data over space and time dimensions, especially incorporating the temporal information into the conventional method, based on Getis-Ord  $G_i^*$  statistics [55] and the Mann-Kendall trend tests [56]. EHSA creates a raster pixel of maps to express the statistically significant clusters of specific elements, using overlays of the temporal and spatial patterns of each corresponding geographical in each year. This method applies to calculating the spatial non-stationarities of precipitation, temperature, NDVI, and DFI. Their long-term change allows us to be known of the locations and extent of past variations. To calculate EHSA, we used the ArcGIS pro2.8 tool and, Create Space Time Cube, to establish spacetime cubes that show the spatial and temporal gridded dataset of the research elements in a network common data form (NetCDF) format. The spacetime cubes of the spatial grid were decided by the spatial resolution, whereas the temporal grid was revealed each year. To create new multi-dimensional raster data for each feature from 1982 to 2020 (the coordinate system is set to the Albers projection, the unit is meters, and the distance unit is calculated more accurately than the geographic coordinates), we added the fields variable (text), dimensions (text) and stdtime (date). Then, a space-time cube (NC format) was created, followed by an analysis of emerging space-time hotspots. Thus, precipitation, temperature, NDVI, and DFI in each temporal and spatial interval were aggregated in these cubes. There were 17 pattern classes of spatial-temporal modes, which are the hot spots and cold spots of new, consecutive, intensifying, persistent, diminishing, sporadic, oscillating, or historical, respectively [57].

#### 2.3.3. Gravity Center Change Mode

Over the last several years, the principle of the population gravity centers has been used to research the moving process of the desertification gravity center [58]. In this

research, the gravity center change model was applied to obtain the NDVI with no detected hotspot gravity center distribution for every month according to Equations (4) and (5) [59]:

$$X_t = \sum_{i=1}^m (C_{ti} \times A_i) / \sum_{i=1}^m (C_{ti}) \tag{4}$$

$$Y_t = \sum_{i=1}^m (C_{ti} \times B_i) / \sum_{i=1}^m (C_{ti}) \tag{5}$$

where  $X_t$  and  $Y_t$  represents the latitude and longitude coordinates of the non- detected hotspot distribution in year  $t$ , respectively;  $C_{ti}$  is the area of the  $i_{th}$  non-detected hotspot in year  $t$ ; and  $A_i$  and  $B_i$  are the longitude and latitude of the gravity plaque center in the  $i_{th}$  non-detected hotspot.

### 2.3.4. DFI

The DFI was summarized according to the MODIS band range and the spectral characteristics of PV, DF, and soil. The formula used is as follows:

$$DFI = 100 \times \left( 1 - \frac{SWIR2}{SWIR1} \right) \times \frac{Red}{NIR} \tag{6}$$

where  $SWIR1$ ,  $SWIR2$ ,  $Red$ , and  $NIR$  represent bands 6 ( $SWIR$ : 1628–1652 nm), 7 ( $SWIR$ : 2105–2155 nm), 1 ( $Red$ : 620–670 nm), and 2 ( $NIR$ : 841–876 nm) of the MODIS, respectively. The DFI has good potential for estimating DF coverage in grassland regions [60].

The above data and methods were used to analyze the impact of vegetation belt movement on wildfires in the Mongolian Plateau over the last 40 years (Figure 2).

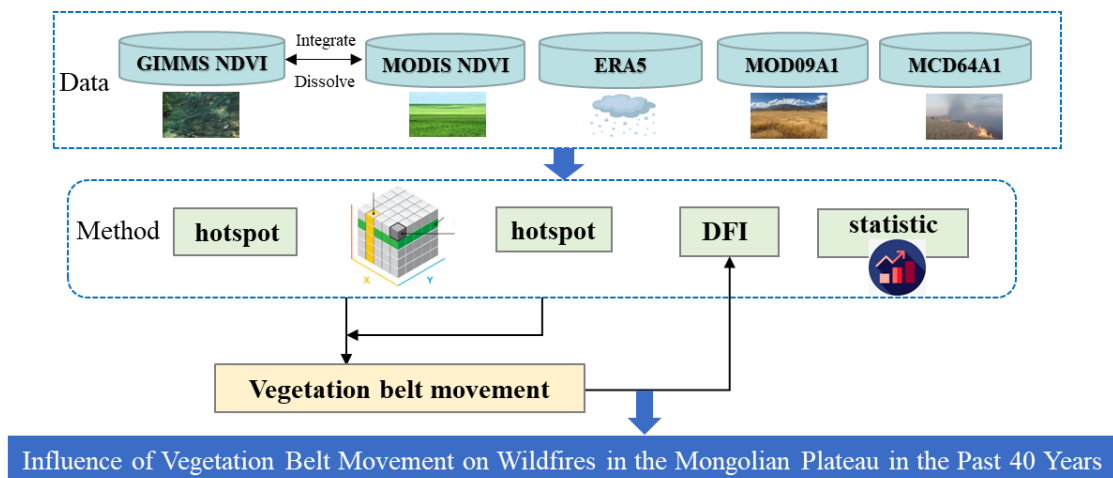
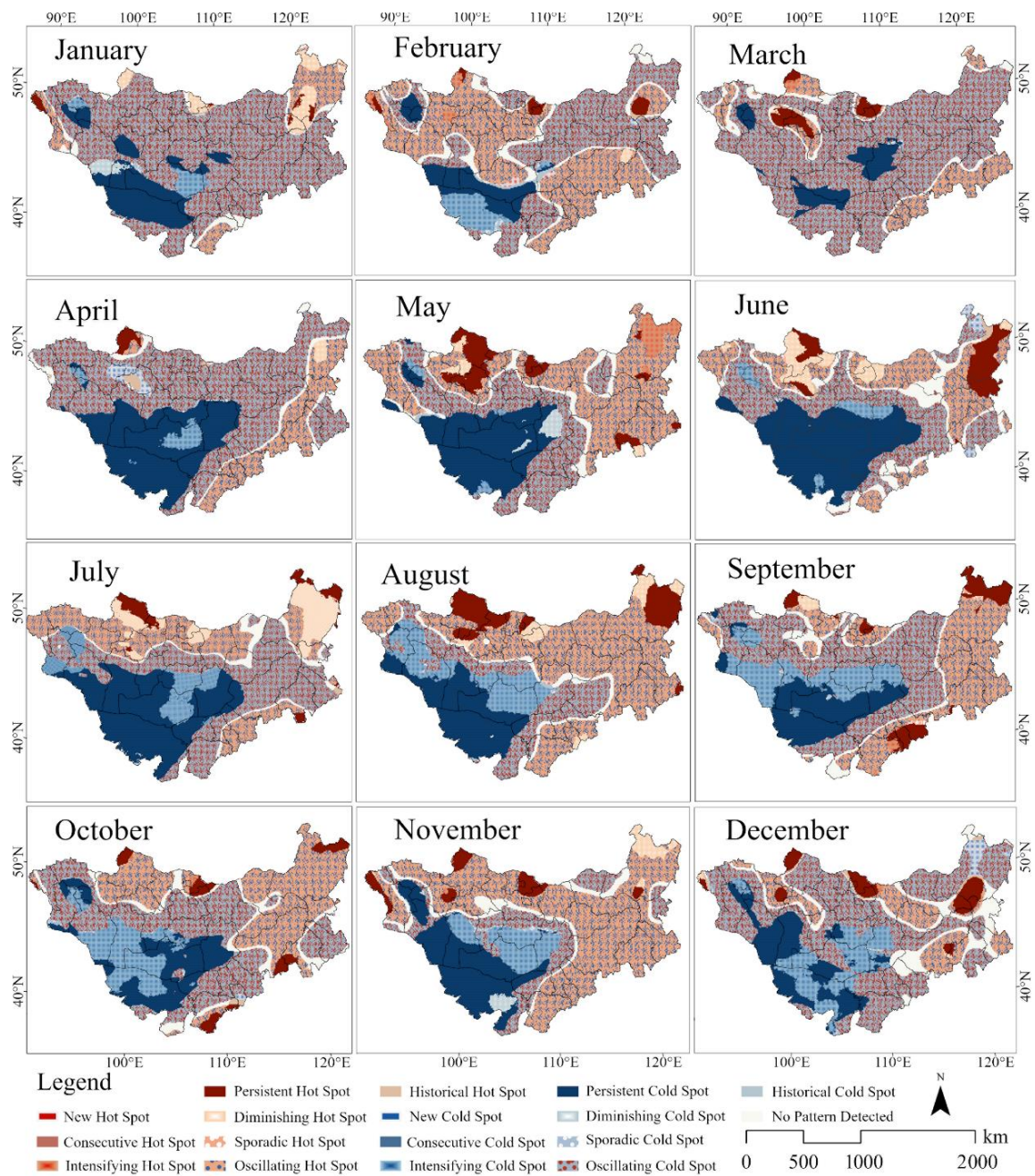


Figure 2. Processing flowchart.

## 3. Result

### 3.1. Analysis of the Variation Patterns of Hydrothermal Conditions over the Mongolian Plateau in the Last 40 Years

The overall precipitation trend was decreasing; in winter, there was a small increase in western Mongolia, and in summer, the eastern sections of the Mongolian Plateau revealed an unsustained increasing trend. Southwest precipitation resulted in a persistent cold spot. The southwest overall was a consecutive cold spot. Oscillating cold spots and hot spots were widely distributed. Persistent hot spots in the northern region were sporadically distributed (Figure 3).



**Figure 3.** Monthly precipitation hotspot map from 1982 to 2020.

The overall temperature trend was upward; and latitudinal zonal changes were evident. The distribution of hot spots at low latitudes, cold spots in the northern Mongolian Plateau, persistent cold spots in the northern portion of the Mongolian Plateau in winter, and a persistent hotspot in the southern portion of the Mongolian Plateau. Overall distribution of hot spots in the southern Mongolian Plateau throughout the year. Overall distribution of cold spots on the northern Mongolian Plateau. The distribution of cold and hot spots in winter latitudes was more obvious (Figure 4).

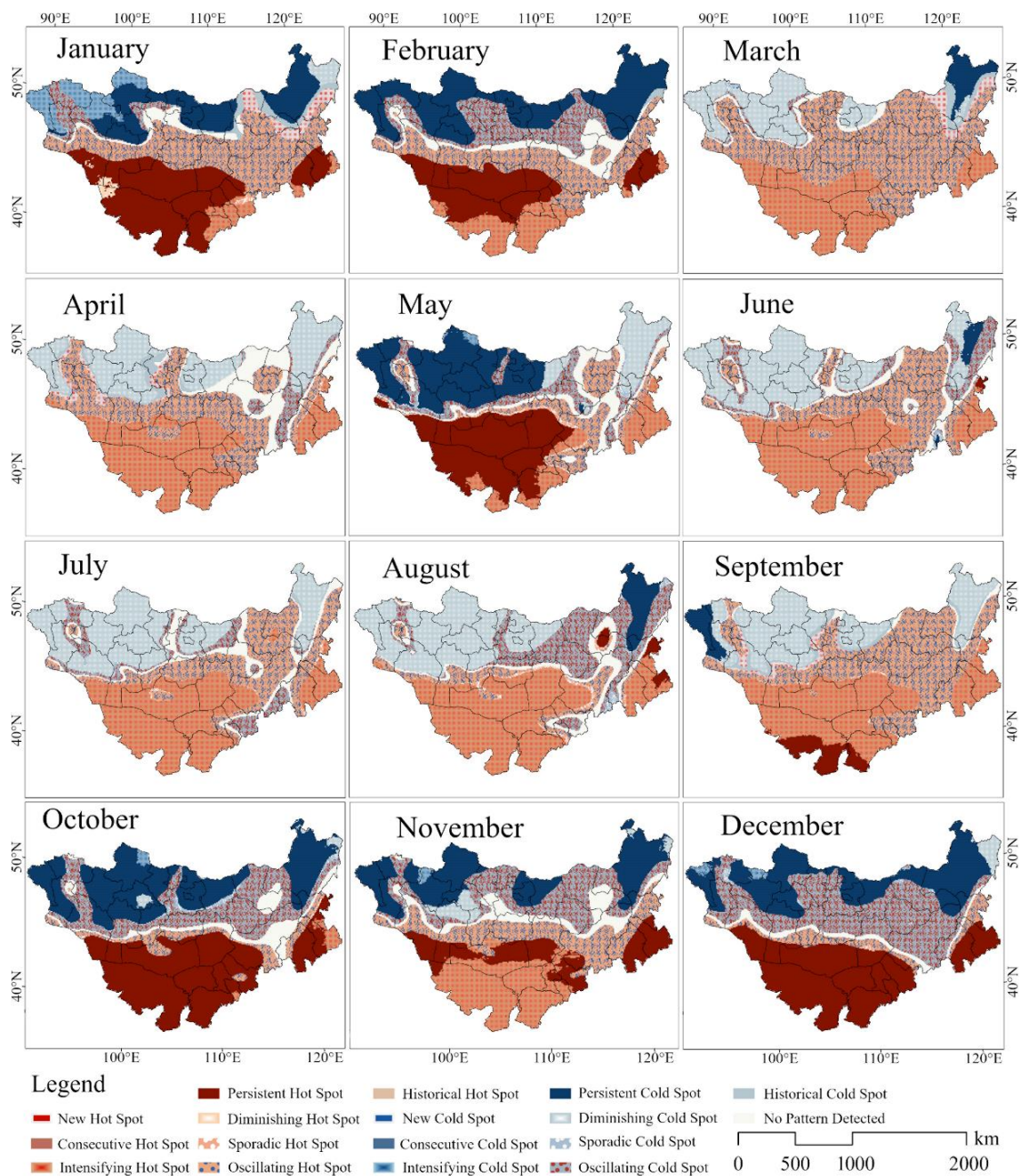


**Figure 4.** Monthly temperature hotspot map from 1982 to 2020.

### 3.2. NDVI Change Patterns and Shifting Characteristics of Vegetation Zones in the Mongolian Plateau in the Last 40 Years

#### 3.2.1. Analysis of NDVI Change Patterns in Mongolian Plateau in the Last 40 Years

The Mongolian Plateau NDVI is the dividing line between the arid and semi-arid areas during the growing season from April to October. It was a hotspot in the northeast, with growth of vegetation decreasing in the southwest and increasing in the northeast, whereas the southwest was a cold spot where vegetation was reduced. An obvious transitional band was observed between the cold spot and the hot spots. The variation in the vegetation index at the regional scale was not significantly related to hydrothermal conditions. This coincided well to the distribution of hydrothermal conditions (Figure 5).

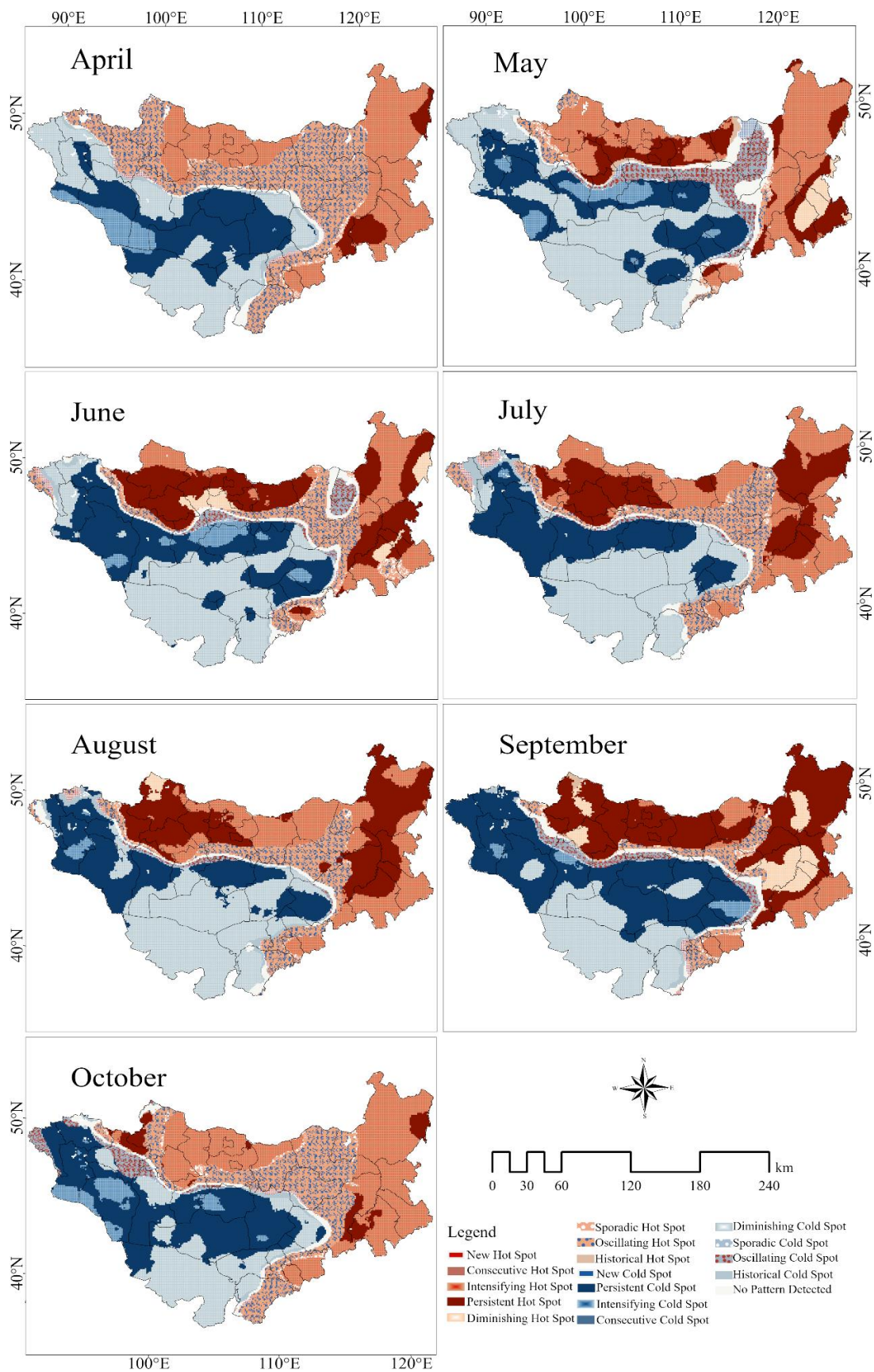


Figure 5. Monthly NDVI hotspot map for 1982–2020.

In the past 40 years, the NDVI movement has varied over the months and the boundary between the hotspot and coldspot NDVI moved. It was more southerly in April, July, and August, southwesterly in April, and was in the northern section of the Mongolian Plateau in May, June, September, and October. The fluctuation in May was large, and in the far northeast, June had the next largest fluctuation. The precipitation was heavy in July and August, and it was close to the southwest desert, and in September and October, it was close to the northeast vegetation area (Figure 6). In terms of longitude, except for May, the longitude decreased with an increase in the month and moved to the western desert area (Figure 7).

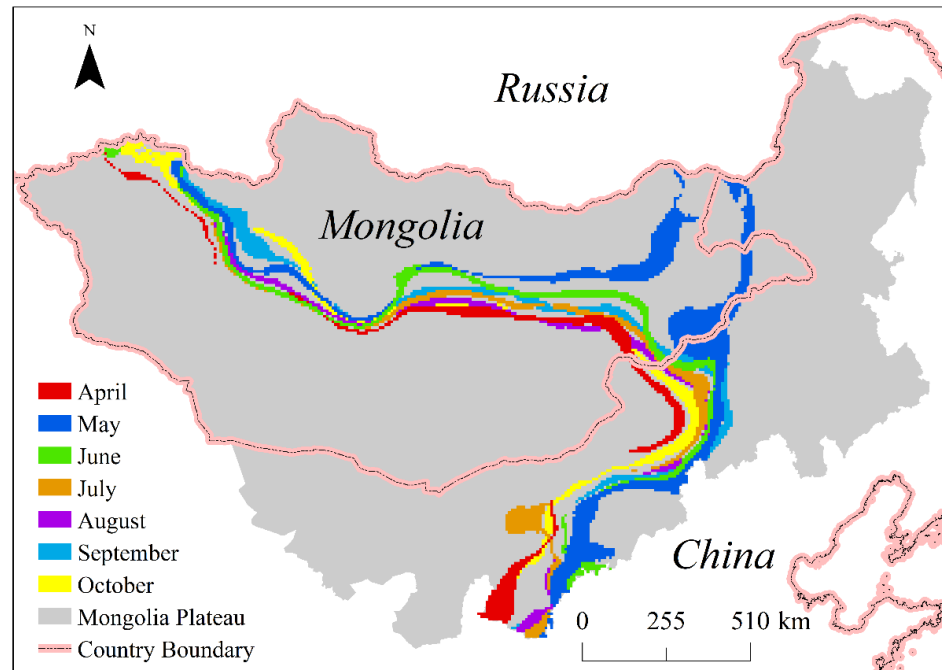


Figure 6. Movement map of hotspots and coldspots in the growing season from 1982 to 2020.

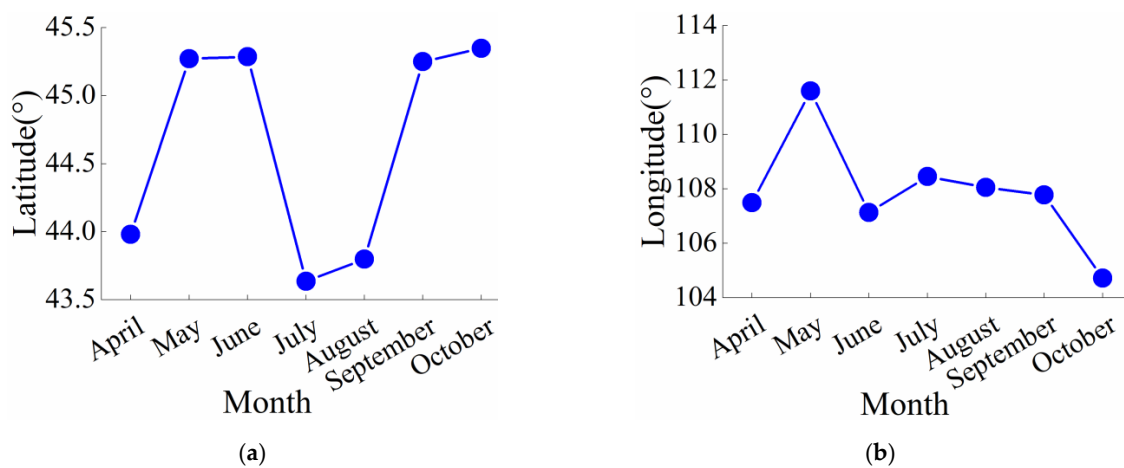
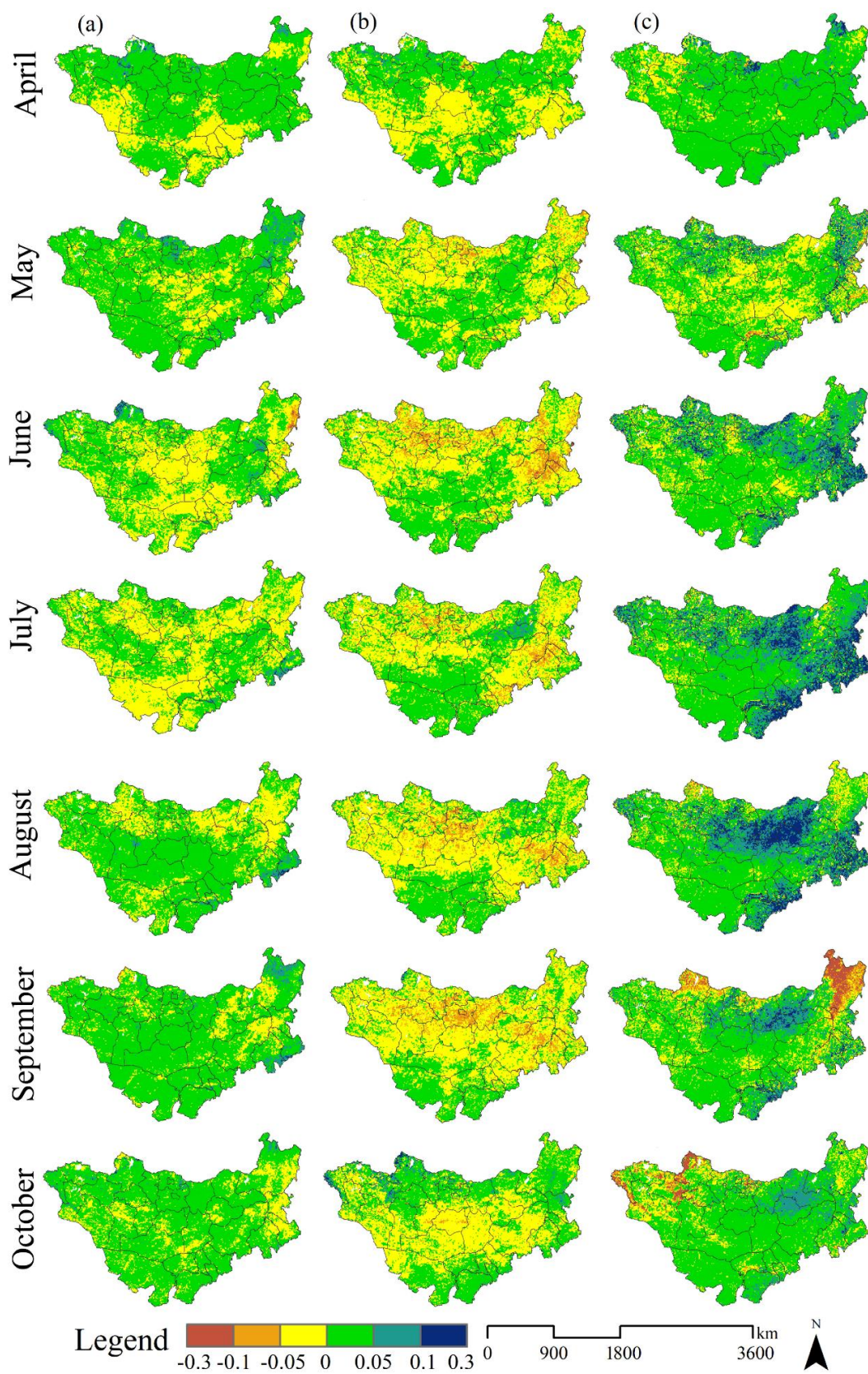


Figure 7. The center point of the no detected line changes in the latitude (a) and longitude (b) in Mongolia Plateau during 1982–2020.

### 3.2.2. Vegetation Belt Movement Features

From 1982–1991 to 1992–2001, 1992–2001 to 2002–2011, and 2012–2020 to 2002–2011, except for the general trend of downward trend–upward trend–upward trend in October, the other growing season months showed an overall trend of upward trend–downward trend–upward trend. (Figure 8).



**Figure 8.** (a) NDVI change for the 1982–1991 period and the 1992–2001 period, (b) NDVI change for the 1992–2001 period and the 2002–2011 period, (c) NDVI change for the 2002–2011 period and the 2012–2020 period.

### 3.3. Effects of Vegetation Belt Movement Characteristics on Wildfire in the Last 40 Years

#### 3.3.1. Analysis of DFI Change Patterns in the Mongolian Plateau from 2000 to 2020

The meadow steppe area had more oscillating hot spots and oscillating cold spots during the withering period, which is also consistent with the volatility of the period. In March, April, May, and June, the oscillating hotspot on the China–Mongolia border area provided favorable conditions for fire occurrence. The distribution regularity of DFI in the withering period was consistent with that of typical grasslands. Hotspots were distributed in the DFI of the northern Mongolian Plateau and the eastern China–Mongolia border area. The northeastern part of Mongolia was characterized by persistent hotspots in April, May, June, and September. The China–Mongolia border areas had persistent hotspots in April, June, September, and October (Figure 9). These months are consistent with fire occurrence in border areas [61].

#### 3.3.2. Relationship between NDVI and Wildfire with Vegetation Zone Change

The withering period in the Mongolian Plateau started in September, and the spatial distribution pattern of the plateau at the end of the growing season (EOS) showed a gradual delay from southwest to northeast and from south to north, which was highly correlated with spatial vegetation productivity [48]. In Central Asia, the withering period is from October to December, but the withering period occurs earlier [62]. From 2002–2011 to 2012–2020 in September, the NDVI increased in the northern Kent Mountains, fires also increased in the northern Kent Mountains from 2011 to 2020, and the fire area expanded (Figure 10). During the withering period from 2002–2011 to 2012–2020 in October, the NDVI in the northern Kent Mountain region increased more than in September, the fires also increased from 2011–2020, and the fire area expanded. Vegetation belts moved northwards; therefore, fires in September and October during the withering period moved northward (Figure 11). This is consistent with the northward shift of the vegetation withering period in September and October [42].

From 2001 to 2015, there were 213 random points in April, May, June, September, and October in the average overlap of the NDVI and DFI, with a total of 1160 sample points. The correlation between NDVI and DFI was significant at the 0.01 level. Therefore, NDVI and DFI were correlated (Figure 12 and Table 1).

#### 3.3.3. Relationship between DFI and wildfire with Vegetation Zone Change

DFI also increased in NDVI-increasing regions and decreased in NDVI-decreasing regions (Figures 8 and 13). However, DFI is more representative of the flammability of a fire [63,64]. From 2001 to 2010, each month the DFI was mainly distributed in northern and central Mongolia, the China–Mongolia border area, the forest-edge meadow grassland area of the Greater Khingan Mountains, and the southern steppe marginal area. Except for November, the DFI distribution area in 2011–2020 was larger than that in 2001–2010, mainly in northern and central Mongolia, the Kent Mountains, the China–Mongolia border area, and the southern steppe marginal area.

The probability of occurrence of a high fire DFI value was between 10 and 30 (Figure 14). Summaries of the DFI and the area of fires had a good linear fitting relationship, and  $R^2$  is 0.9964 (Figure 15), using the 33 number of burned area cases. To study hotspots, a symmetrical value of 20–30 was assigned to between 20 and 10, and the probability of fire between 10 and 20 increased. The fire area and DFI trended to be between 10 and 20 (Figure 16).

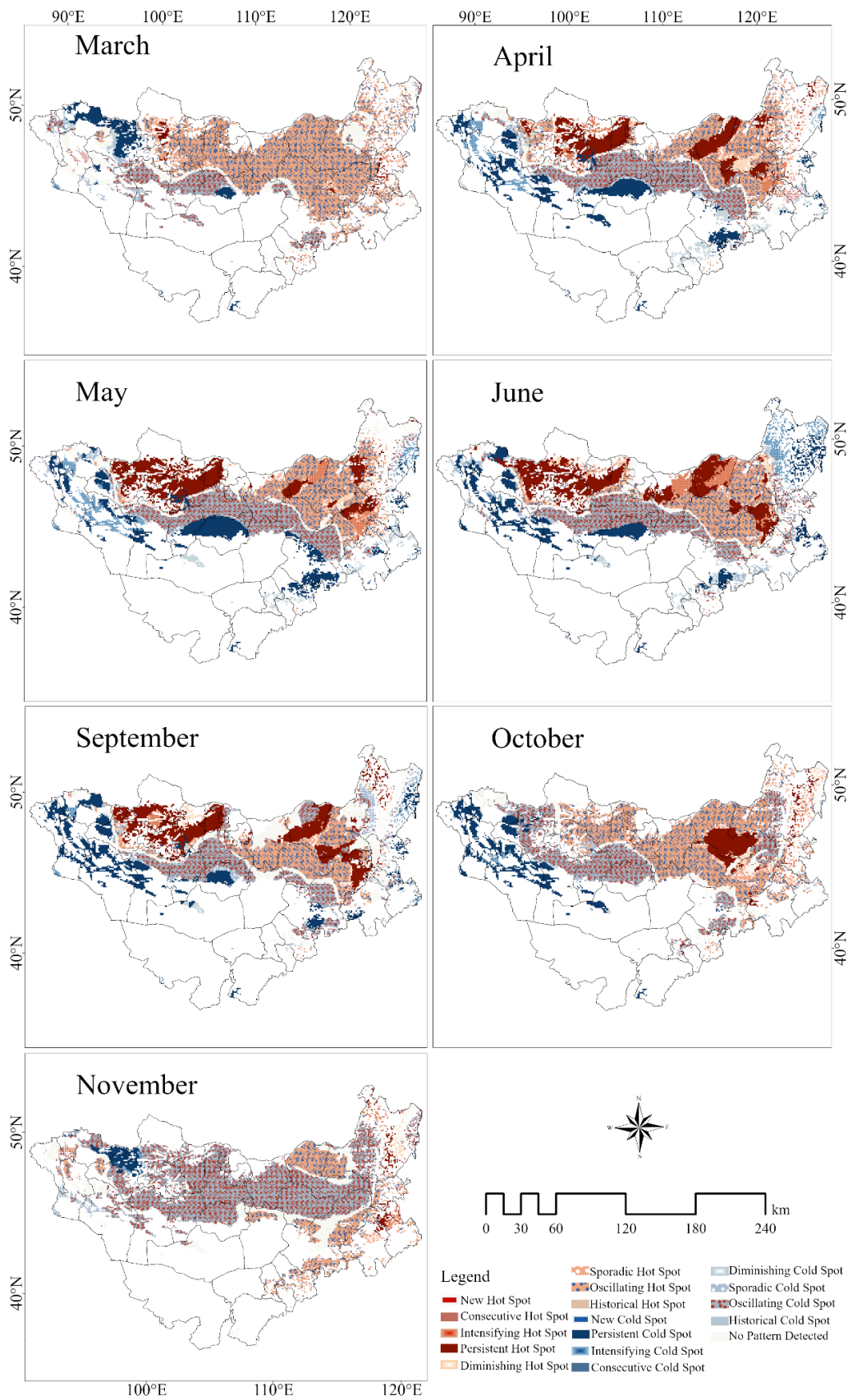
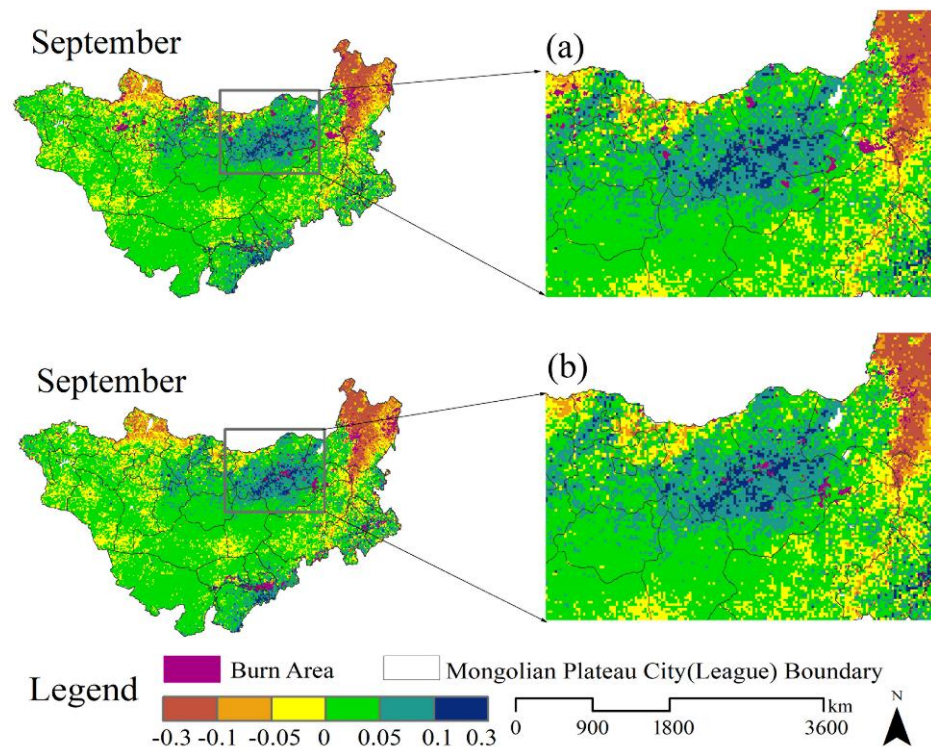
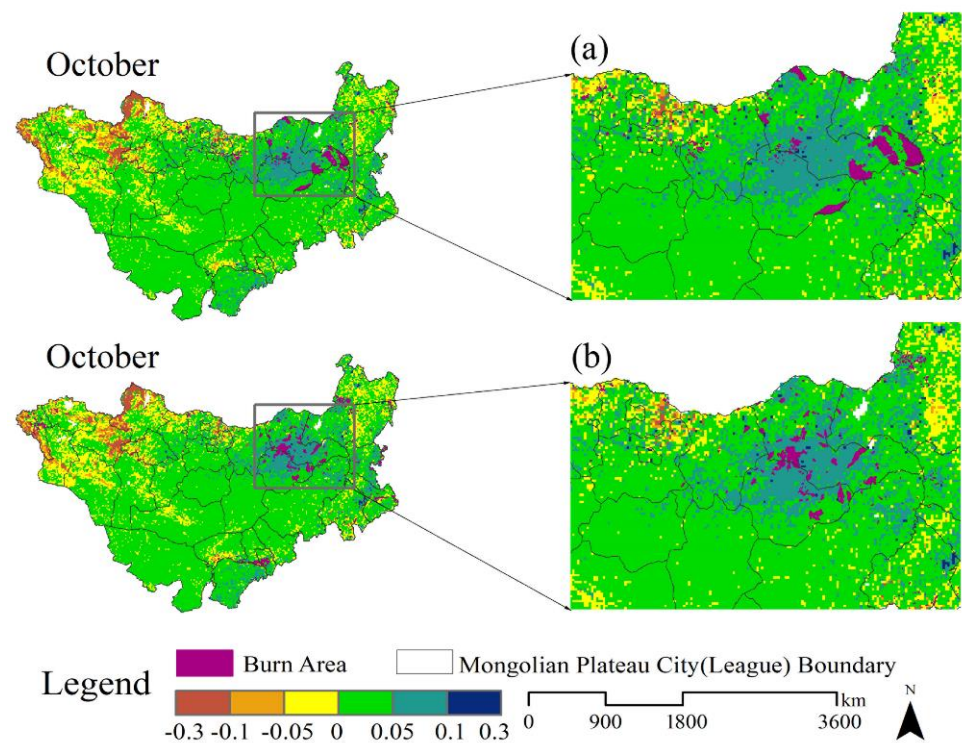


Figure 9. DFI hotspot map during the withering period in the grassland area from 2000 to 2020.



**Figure 10.** NDVI changes in the 2001–September 2010 period and the 2011–September 2020 period, and (a) the area of burned areas from 2001 to 2010 and (b) the area of burned areas from 2011 to 2020.



**Figure 11.** NDVI changes in the 2001–October 2010 period and the 2011–October 2020 period, and (a) the area of burned areas in 2001–2010 and (b) the area of burned areas in 2011–2020.

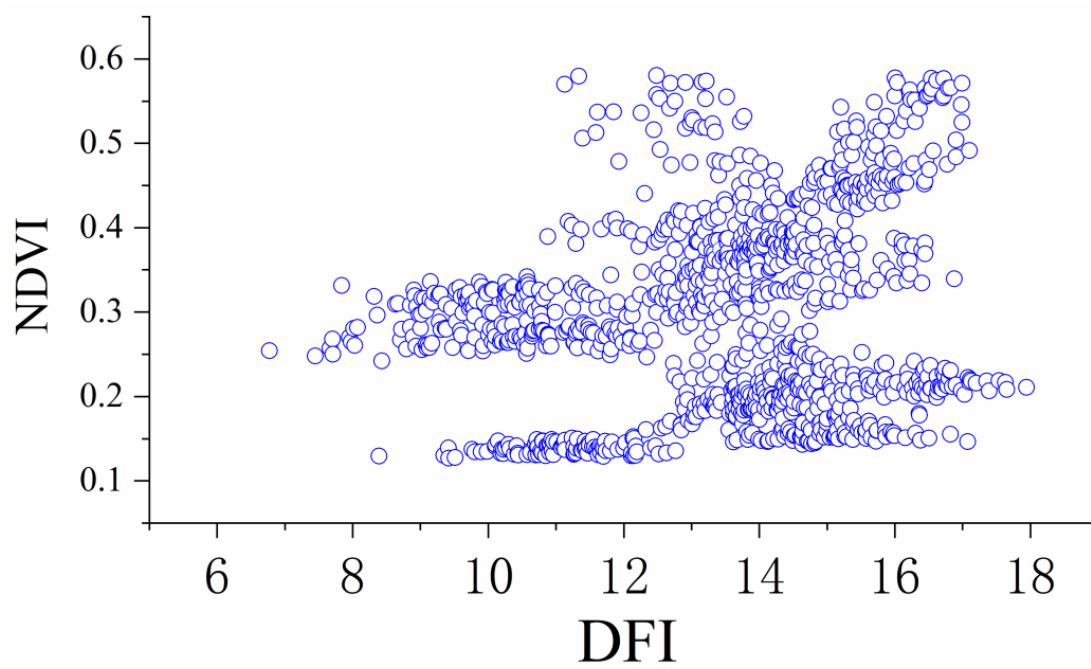


Figure 12. Relationship between NDVI and DFI.

Table 1. Correlation between NDVI and DFI.

NDVI \ DFI	Number of Samples	Person Correlation
	1160	0.193 **

\*\* Significant correlation at the 0.01 level (two-tailed).

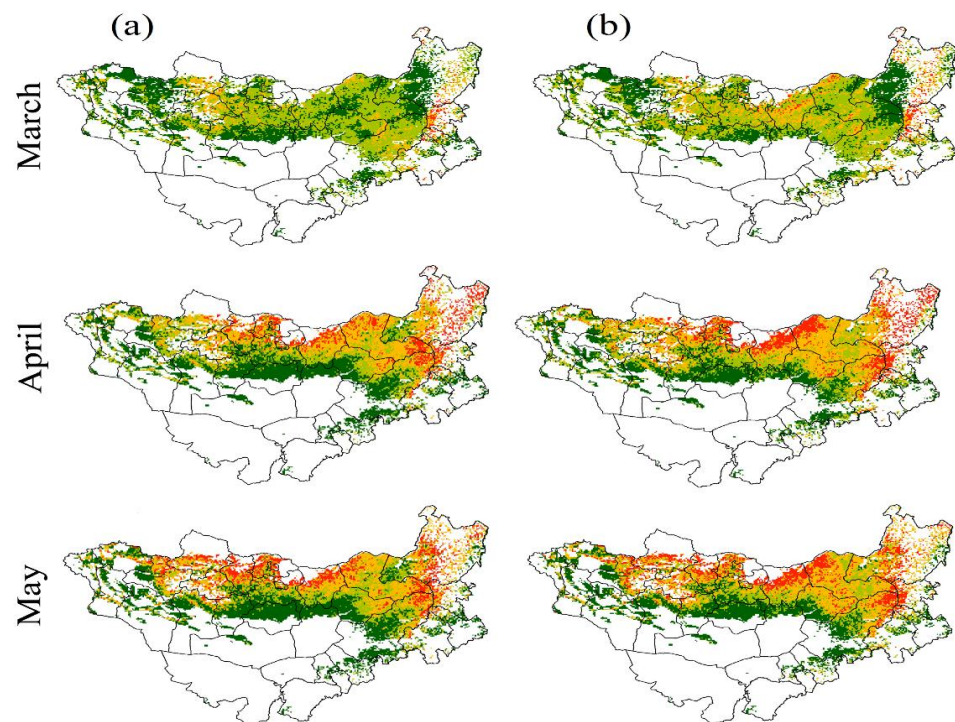


Figure 13. Cont.

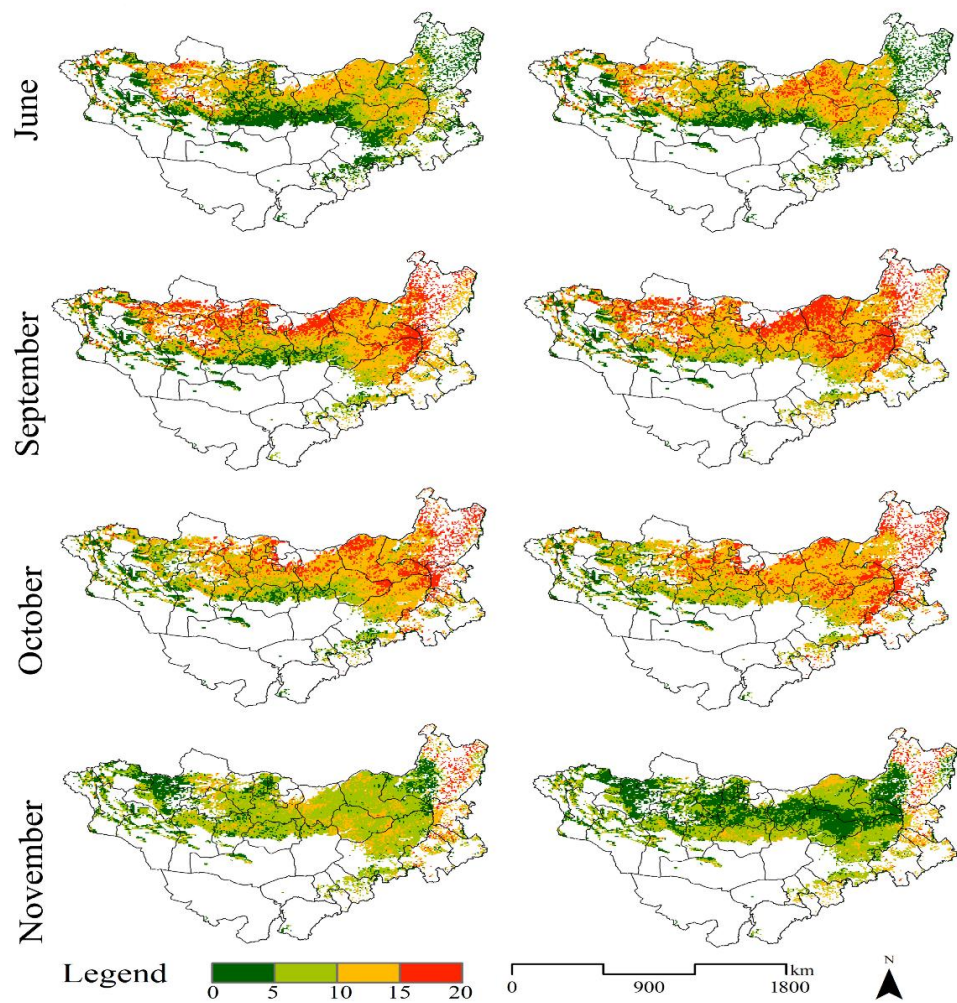


Figure 13. (a) Average DFI of 2001–2010, (b) Average DFI of 2011–2020.

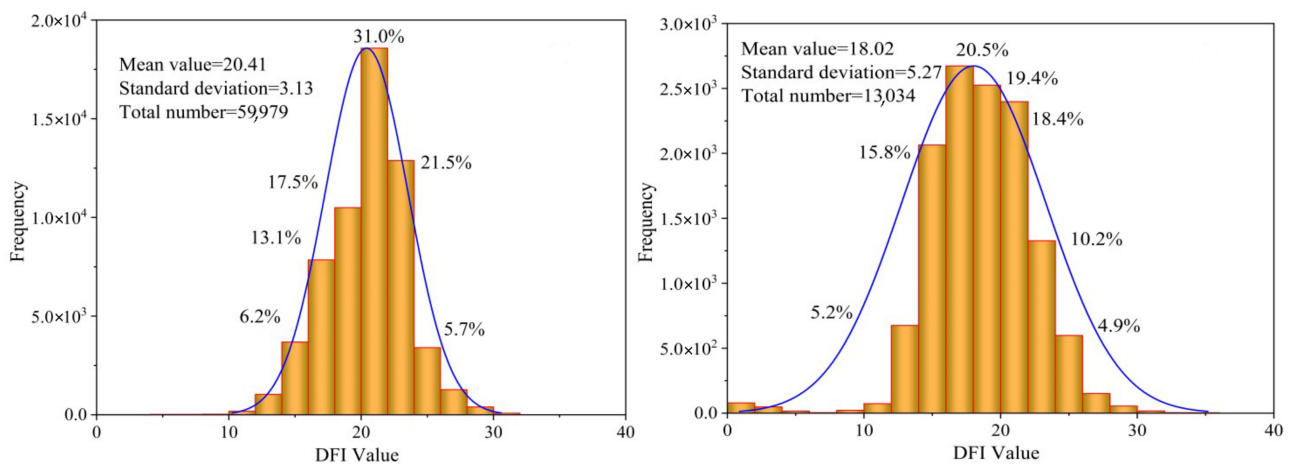


Figure 14. Spatial distributions of annual mean DFI in the study area during 2001–2020.

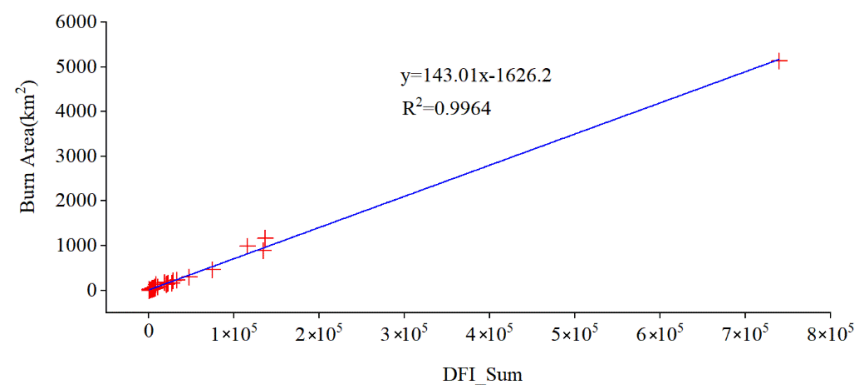


Figure 15. A linear fitting relationship of summarize of DFI and area of fires.

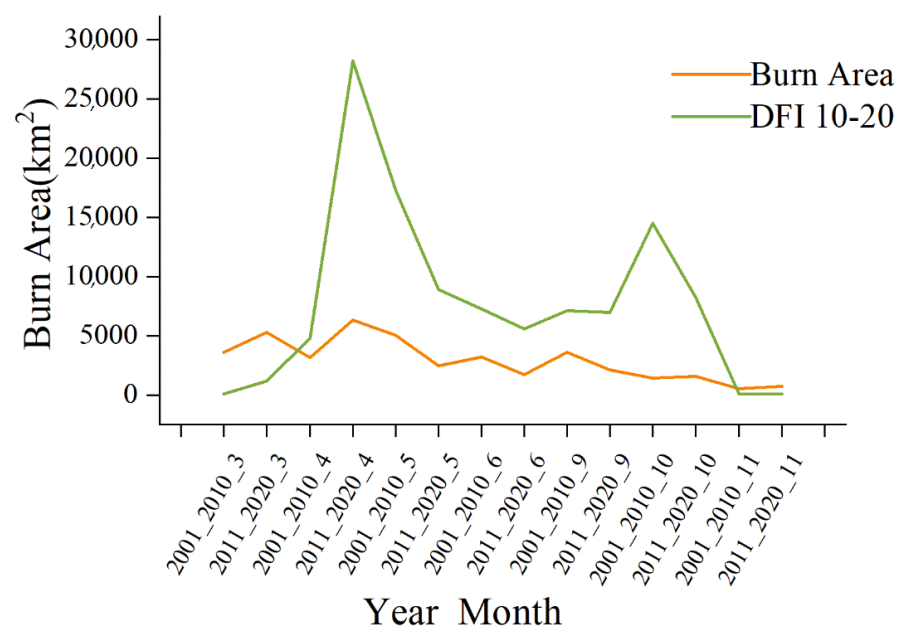


Figure 16. Relationship between DFI and fire area.

## 4. Discussion

### 4.1. NDVI and Hydrothermal Conditions

The boundary between arid and semi-arid regions is consistent with an average annual precipitation of approximately 200 mm, which is also a no-detection line. NDVI increased northeast of the no-detection line and decreased in the southwest. This is because the northern Mongolian Plateau is influenced by Arctic Ocean water vapor, the eastern part is affected by Pacific Ocean water vapor, and water vapor from the Indian Ocean encounters the Himalayas. The annual total precipitation is about 300–400 mm, and with the increase in the distance from the ocean, the precipitation decreases from east to west and from north to south by degrees. Therefore, the hygrometric conditions in the southwestern Mongolian Plateau decrease and are less humid as it is difficult for ocean surface water vapor to reach that far, and has a minimum precipitation of approximately 100 mm. The distribution of air temperature corresponds to the amount of precipitation, with relatively low temperatures in the northern and eastern humid regions, and relatively high temperatures in the southwestern arid regions. This zonal distribution of dryness and humidity coincided with the transitional area shape detected by the NDVI hotspots in this study (Figure 6). Precipitation increased in the northeast and decreased in the southwest during the growing season, and the air temperature decreased in the northeast and increased in the southwest (Figures 3 and 4).

The correlation of precipitation on the Mongolian Plateau from May to August was higher than that of the temperature, and the correlation of temperatures in March, April, September, and October was higher than that of the precipitation (Figures 3–5, 17 and 18). This shows that during the plant growth period, the influence of precipitation on vegetation growth is greater than the effect of temperature [42,65], thus providing unfavorable conditions for fire occurrence. It is consistent with the plant growth period fire occurrence being less than the withering period fire occurrence. More precipitation will lead to more soil moisture, and vegetation moisture, providing unfavorable conditions for fires. Precipitation in May, June, and July exhibited a significant positive correlation with temperature in the northeast (Figures 17 and 18). As a result, the vegetation in the northeast increased. Between precipitation and NDVI had higher correlation than that between NDVI and temperature in arid and semi-arid regions [66].

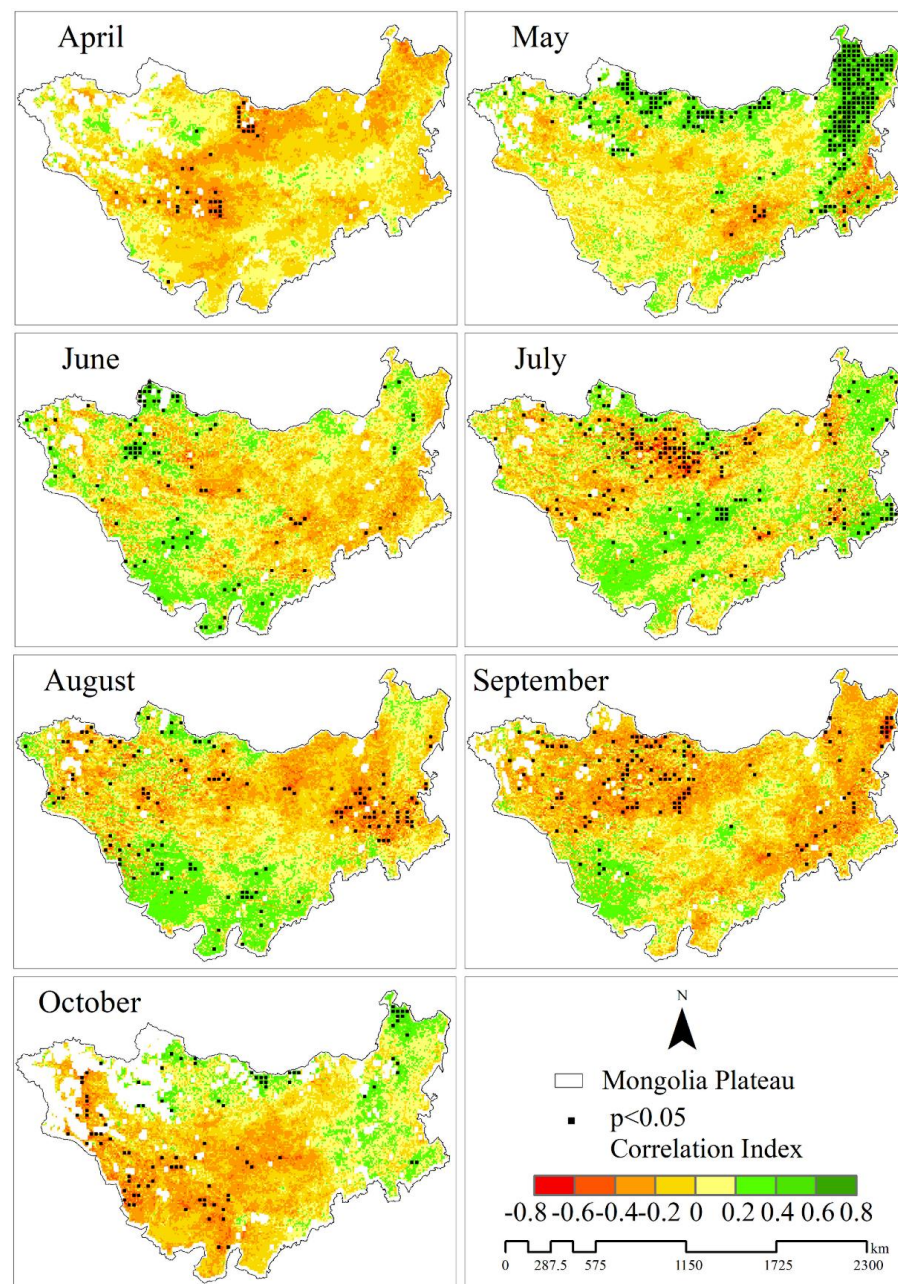
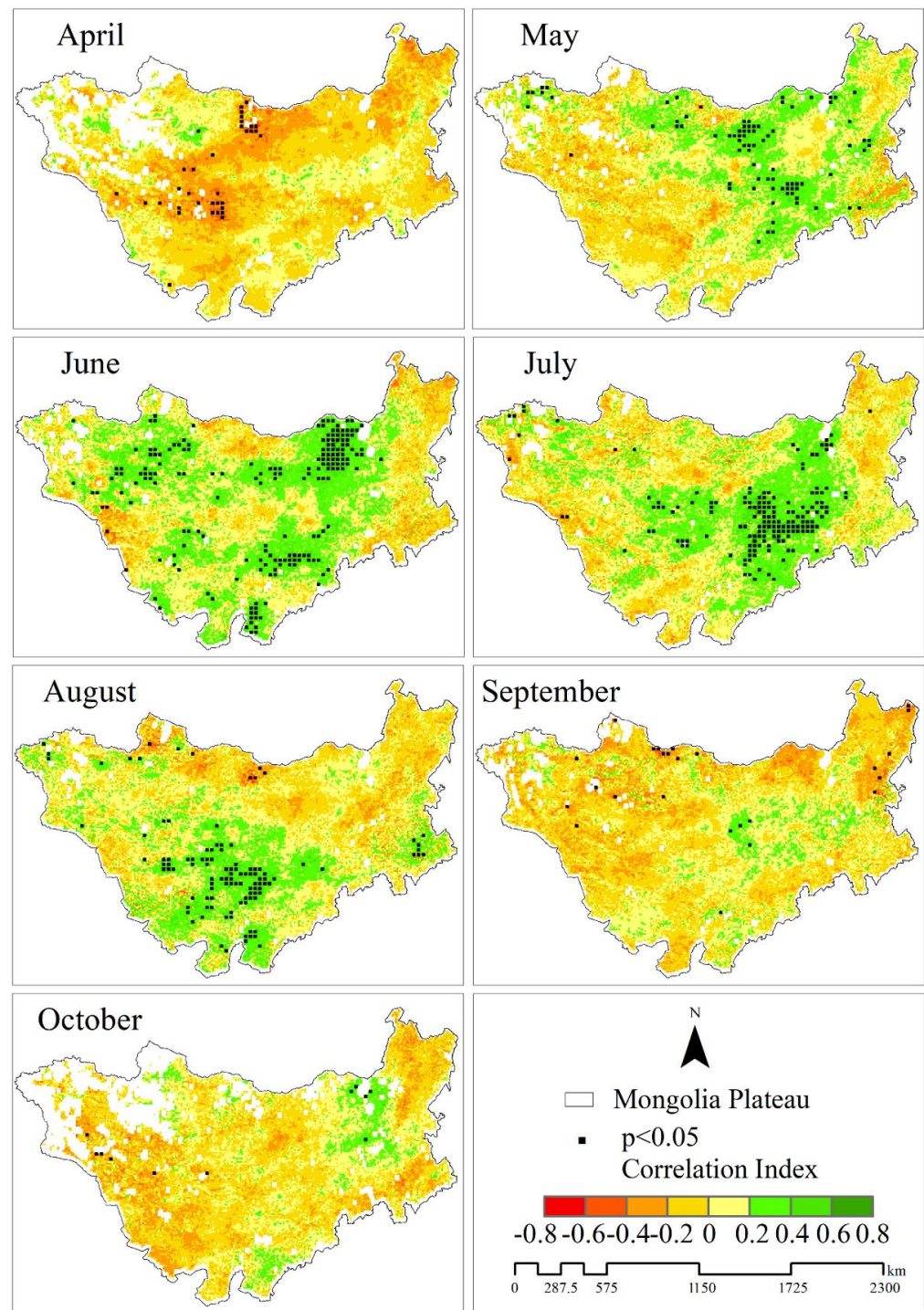


Figure 17. Correlation between NDVI and air temperature from April to October.



**Figure 18.** Correlation between NDVI and precipitation from April to October.

#### 4.2. NDVI and DFI Movement Distribution

The increase in NDVI occurred near the Kent Mountains in northern Mongolia (Figure 5). Against the background of climate warming over the past 40 years, the temperature and precipitation increased in the northern region during the growing season from April to October (Figures 3 and 4). The Dornod, Sukbaatar, Hentiy, and Dornogovi provinces near the Kent Mountains in northern Mongolia have more national reserves and less population distribution, largely confined to the Dornod Mongol Strictly Protected Areas of the Eastern Mongolian Grassland Nature Reserve in Mongolia, mainly on hills and plains [67]. The Daur National Nature Reserve in Haorotu Sumu of Dornod Province

is sparsely populated [68,69], and its natural and geographical environment has not been polluted or damaged by human activities. It has maintained its original natural appearance and abundant pasture resources. Other protected areas include the Nomrog strictly protected area, Daguuriin Mongol—a strictly protected area, Daguuriin Mongol—b strictly protected area, and Nomrog Mnt. strictly protected areas, as well as the Ugtam Mnt. Nature Reserves, Toson Khulstai Nature Reserves, and Lkhachinvandad Mnt. Nature Reserves. The NDVI-DFI response spaces of the image are basically triangles, which conforms to the basic assumption of the linear unmixing model [70,71].

The DFI also increased in northern Mongolia, the China-Mongolia border area, and the forest-edge meadow steppe region of the Great Khingan Mountains. Because of the increase in northern Mongolia, there are more national protected areas [68,69], and the DFI increases due to policy management and less population and livestock in the China-Mongolia border area. The forest margin meadows in the Greater Khingan Mountains are mainly distributed on higher terrain, mostly at an elevation of 700–1500 m, with a relative mountain height difference of 200–300 m [72]. In the Hulunbuir forest-edge meadows of the Greater Khingan Mountains, a forage base was established on the retired farmland with a small slope, a thick soil layer, and good soil [73]. Therefore, the increase in the meadow steppe area of the Greater Khingan Mountains means that grassland protection in the forest edge areas at higher elevations is better.

#### 4.3. NDVI and DFI Movement Distribution and the Relationship between Fires

Combustibles are the basic factors in the formation and spread of grassland fires [36]. The areas where NDVI and DFI increased movement also increased in fire area (Figures 10, 11, 15 and 16). In the absence of meteorological factors and fire sources, the basis of fires was combustibles, and the number of combustibles increased. Thus, fire occurrences were more likely. NDVI can reflect surface vegetation coverage and growth conditions, and DFI is the DF index, which expresses flammable withered grass and is closely related to fire occurrence [74–76]. The fire intensity increases with the ground fuel load [30]. The fuel spatial and variability characterization of the fuel density influences simulated fire behavior [76,77]. Lots of fuel drought as a result of climate change increases fuel availability, as responded to the exponential relationship between fuel dryness and the fire area [23]. From June to August, the NDVI increased more near the Kent Mountains in northern Mongolia (Figure 8c), and the fire area also increased during the dry and withering periods in September and October.

NDVI movement affects fires, with a high NDVI value and fire rate, and can replace combustibles, fuel, weather, and terrain to express the grassland fire basic environment. The fuel load is an elementary factor for the component and spread of grassland fires. For large area of grasslands fire, NDVI can describe fuel load. Many researchers have reflected that field survey and NDVI can be used to create a relationship with fuel load and satellite data [78], as figured up by the following functions [79]: when the value is between 0~0.1, it shows rocks, soil, or aging vegetation; when the value is above 0.1, it represents the existing biomass; when the value is above 0.9, it expresses that the vegetation has a high fuel load and continuity. The closer, approximately the NDVI index value is to 1, the greater the fuel load and continuity [36,75]. Hernandez-Leal defined the Fire Risk Dynamic Index using AVHRR data and the NDVI [80].

Fire protection is difficult in the border areas of China and Mongolia, and grasslands are widely distributed, Khalkgol, Erdenetsagaan, and Matad in Mongolia and East Ujumqin Banner in China have the highest occurrence rate of grassland fires, and there is more ground fuel [35]. The growing season NDVI in the border areas of China and Mongolia increased, and the growing season NDVIs in Inner Mongolia and Mongolia were 0.0018/a and 0.0021/a, respectively [67]. It is consistent with the increase in NDVI and DFI, which caused the occurrence of fire in the border area of China and Mongolia. Fires decreased after sheep grazing in the Navajo-Ponderosa pine forest [81]. Between the 30 and 40 latitudes, the withering period was earlier [82], moved northward, and yellowed earlier,

while the amount of dry grass increased, and the yellowing period in North America was prolonged [83]. In most areas of Asia south of 55° N, the EOS is often delayed by more than 0.25 days /year [84]. The above conclusion is consistent with this study's point that the withering period has been prolonged, and the amount of dry grass increased. Therefore, the probability of fire is also high. More fires happen in October (Figures 11 and 16). The relationship between the DFI and the area of the fire area is consistent (Figure 16), and fire occurrence is accidental. The environment (meteorological elements, terrain, etc.) interacts with the fire occurrence and area, but the fire source is accidental, and the acquisition of a fire environment is relatively simple; however, combustibles are more complicated factors [85–87]. This study only examined the impact of DFI on fire from one side, and not the combustibles, meteorological elements, and fire sources when a fire occurs to explain fire probability.

## 5. Conclusions

Vegetation in cold environments, such as those in the mid-to-high latitudes and high elevations, moves to higher latitudes or elevations in response to global warming. The fuel distribution changes with climate change. The Mongolian Plateau is bound by arid and semi-arid regions. Over the past 40 years, the vegetation in the southwest has decreased, and the vegetation in the northeast has increased. With the northward movement of vegetation on the Mongolian Plateau, fire occurrence has also moved northward, especially in the nearby Kent Mountains and concentrated in Dornod, Sukhbaatar, and Kent provinces, which has become more obvious in the past 20 years. The probability of DFI fires is high in northern Mongolia, the border areas between China and Mongolia, and the forest-edge meadow steppe region of the Greater Khingan Mountains. These findings suggest that vegetation is migrating northward because of climate change and presents a challenge of future warming spreading fire northward, adding material to the study of the relationship between the northward movement of global vegetation and fires.

**Author Contributions:** L.C. conceptualization, methodology, data curation, writing-original draft; J.Z. Conceptualization, Supervision, Writing-reviewing and editing; Y.B. (Yulong Bao) Conceptualization, Funding acquisition, Writing-reviewing and editing; Y.B. (Yuhai Bao) supervision; L.M. and E.C. software, writing-review and editing. All authors have read and agreed to the published version of the manuscript.

**Funding:** This study was financially supported by the International (Regional) Cooperation and Exchange Programs of National Natural Science Foundation of China (41961144019), the Natural Science Foundation of Inner Mongolia Autonomous Region (2021MS04016), the Major Scientific and Technological Program of Inner Mongolia Autonomous Region (2021ZD004503), the Key R&D and Achievement Transformation Program of Inner Mongolia Autonomous Region (2022YFSH0070), the Key R&D Social Public Field and Achievement Transformation Plan Project in the 14th Five Year Plan of Inner Mongolia Autonomous Region (2022YFSH0132) and the Key Philosophy and social science program of Inner Mongolia Autonomous Region (2022NDA225).

**Data Availability Statement:** Not applicable.

**Conflicts of Interest:** The authors declare no conflict of interest.

## References

1. Løkken, J.O.; Evju, M.; Söderström, L.; Hofgaard, A. Vegetation response to climate warming across the forest–tundra ecotone: Species-dependent upward movement. *J. Veg. Sci.* **2020**, *31*, 854–866. [[CrossRef](#)]
2. Pecl, G.T.; Araújo, M.B.; Bell, J.D.; Blanchard, J.; Bonebrake, T.C.; Chen, I.-C.; Clark, T.D.; Colwell, R.K.; Danielsen, F.; Evengård, B.; et al. Biodiversity redistribution under climate change: Impacts on ecosystems and human well-being. *Science* **2017**, *355*, 1389. [[CrossRef](#)] [[PubMed](#)]
3. Hansson Amanda, D.P.; Jamie, S. A review of modern treeline migration, the factors controlling it and the implications for carbon storage. *J. Mt. Sci.* **2021**, *18*, 291–306. [[CrossRef](#)]
4. Harsch, M.A.; Hulme, P.E.; McGlone, M.S.; Duncan, R. Are treelines advancing? A global meta-analysis of treeline response to climate warming. *Ecol. Lett.* **2009**, *12*, 1040–1049. [[CrossRef](#)]

5. Mekonnen, Z.A.; Riley, W.J.; Berner, L.T.; Bouskill, N.J.; Torn, M.S.; Iwahana, G.; Breen, A.L.; Myers-Smith, I.H.; Criado, M.G.; Liu, Y.; et al. Arctic tundra shrubification: A review of mechanisms and impacts on ecosystem carbon balance. *Environ. Res. Lett.* **2021**, *16*, 053001. [[CrossRef](#)]
6. Anne, E.; Kelly, M.L.G. Rapid shifts in plant distribution with recent climate change. *Proc. Natl. Acad. Sci. USA* **2008**, *105*, 11823–11826.
7. Crimmins, S.M. Changes in climatic water balance drive downhill shifts in plant species' optimum elevations. *Science* **2011**, *331*, 324–327. [[CrossRef](#)]
8. Liang, Q.; Xu, X.; Mao, K.; Wang, M.; Wang, K.; Xi, Z.; Liu, J. Shifts in plant distributions in response to climate warming in a biodiversity hotspot, the Hengduan mountains. *J. Biogeogr.* **2018**, *45*, 1334–1344. [[CrossRef](#)]
9. Oliveira, U.; Soares-Filho, B.; Costa, W.L.d.S.; Gomes, L.; Bustamante, M.; Miranda, H. Modeling fuel loads dynamics and fire spread probability in the Brazilian cerrado. *For. Ecol. Manag.* **2021**, *482*, 118889. [[CrossRef](#)]
10. Bowman, D.M.; Kolden, C.A.; Abatzoglou, J.T.; Johnston, F.H.; van der Werf, G.R.; Flannigan, M. Vegetation fires in the anthropocene. *Nat. Rev. Earth Environ.* **2020**, *1*, 500–515. [[CrossRef](#)]
11. Chen, Y.; Romps, D.M.; Seeley, J.T.; Veraverbeke, S.; Riley, W.J.; Mekonnen, Z.A.; Randerson, J.T. Future increases in arctic lightning and fire risk for permafrost carbon. *Nat. Clim. Change* **2021**, *11*, 404–410. [[CrossRef](#)]
12. Liu, M.; Yang, L. Northward expansion of fire-adaptive vegetation in future warming. *Environ. Res. Lett.* **2022**, *17*, 024008. [[CrossRef](#)]
13. Carlson, J.D.; Burgan, R.E. Review of users' needs in operational fire danger estimation: The Oklahoma example. *Int. J. Remote Sens.* **2010**, *24*, 1601–1620. [[CrossRef](#)]
14. Ping, G.; Chunli, K.; Wei, T. Relationship between the characteristics of fuel bed and fire behavior in grassland. *Arid Zone Res.* **2002**, *19*, 13–16.
15. Zheng, H.; Ju, E.; Chai, R.; Du, X. *Forest Fire Management*; Press of Northeast Forestry University: Harbin, China, 1988; pp. 5–10.
16. Li, Y.; Wang, S. Response of plant and plant community to different stocking rates. *Grassl. China* **1999**, *3*, 11–19.
17. Li, H.; Pan, H.; Wang, G. Degradation causes of typical steppe in Inner Mongolia. *Pratacultural Sci.* **2004**, *21*, 49–51.
18. Wang, S.-P.; Li, Y.-H.; Wang, Y.-F.; Chen, Z.-Z. Influence of different stocking rates on plant diversity of artemisia frigida community in Inner Mongolia steppe. *Acta Bot. Sin.* **2001**, *43*, 89–96.
19. Taneja, R.; Hilton, J.; Wallace, L.; Reinke, K.; Jones, S. Effect of fuel spatial resolution on predictive wildfire models. *Int. J. Wildland Fire* **2021**, *30*, 776–789. [[CrossRef](#)]
20. Hurteau, M.D.; Liang, S.; Westerling, A.L.; Wiedinmyer, C. Vegetation-fire feedback reduces projected area burned under climate change. *Sci. Rep.* **2019**, *9*, 2838. [[CrossRef](#)]
21. Hanan, E.J.; Kennedy, M.C.; Ren, J.; Johnson, M.C.; Smith, A.M.S. Missing climate feedbacks in fire models: Limitations and uncertainties in fuel loadings and the role of decomposition in fine fuel accumulation. *J. Adv. Model. Earth Syst.* **2021**, *14*, 2818. [[CrossRef](#)]
22. Riley, K.L.; Williams, A.P.; Urbanski, S.P.; Calkin, D.E.; Short, K.C.; O'Connor, C.D. Will landscape fire increase in the future? A systems approach to climate, fire, fuel, and human drivers. *Curr. Pollut. Rep.* **2019**, *5*, 9–24. [[CrossRef](#)]
23. Davis, C. Earth, fuel and fire. *Nat. Rev. Earth Environ.* **2021**, *2*, 742. [[CrossRef](#)]
24. Abatzoglou, J.T.; Battisti, D.S.; Williams, A.P.; Hansen, W.D.; Harvey, B.J.; Kolden, C.A. Projected increases in western US forest fire despite growing fuel constraints. *Commun. Earth Environ.* **2021**, *2*, 227. [[CrossRef](#)]
25. Calviño-Cancela, M.; Lorenzo, P.; González, L. Fire increases eucalyptus globulus seedling recruitment in forested habitats: Effects of litter, shade and burnt soil on seedling emergence and survival. *For. Ecol. Manag.* **2018**, *409*, 826–834. [[CrossRef](#)]
26. van der Werf, G.R.; Randerson, J.T.; Giglio, L.; van Leeuwen, T.T.; Chen, Y.; Rogers, B.M.; Mu, M.; van Marle, M.J.E.; Morton, D.C.; Collatz, G.J.; et al. Global fire emissions estimates during 1997–2016. *Earth Syst. Sci. Data* **2017**, *9*, 697–720. [[CrossRef](#)]
27. John, T.; Abatzoglou, A.P.W. Impact of anthropogenic climate change on wildfire across western US forests. *Proc. Natl. Acad. Sci. USA* **2016**, *113*, 11770.
28. Carol Miller, D.L.U. Connectivity of forest fuels and surface fire regimes. *Landsc. Ecol.* **2000**, *15*, 145–154. [[CrossRef](#)]
29. Juli, G.; Pausas, S.P. Fuel shapes the fire–climate relationship: Evidence from Mediterranean ecosystems. *Glob. Ecol. Biogeogr.* **2012**, *21*, 1074–1082.
30. Sah, J.P.; Ross, M.S.; Snyder, J.R.; Koptur, S.; Cooley, H.C. Fuel loads, fire regimes, and post-fire fuel dynamics in Florida keys pine forests. *Int. J. Wildland Fire* **2006**, *15*, 463–478. [[CrossRef](#)]
31. Syphard, A.D.; Radeloff, V.C.; Keeley, J.E.; Hawbaker, T.J.; Clayton, M.K.; Stewart, S.I.; Hammer, R.B. Human influence on California fire regimes. *Ecol. Appl.* **2007**, *17*, 1388–1402. [[CrossRef](#)]
32. Balch, J.K.; Bradley, B.A.; Abatzoglou, J.T.; Nagy, R.C.; Fusco, E.J.; Mahood, A.L. Human-started wildfires expand the fire niche across the United States. *Proc. Natl. Acad. Sci. USA* **2016**, *114*, 2946–2951. [[CrossRef](#)]
33. Tong, S.; Zhang, J.; Bao, Y.; Lai, Q.; Lian, X.; Li, N.; Bao, Y. Analyzing vegetation dynamic trend on the Mongolian plateau based on the Hurst exponent and influencing factors from 1982–2013. *J. Geogr. Sci.* **2018**, *28*, 595–610. [[CrossRef](#)]
34. Bao, G.; Qin, Z.; Bao, Y.; Zhou, Y.; Li, W.; Sanjiv, A. NDVI-based long-term vegetation dynamics and its response to climatic change in the Mongolian plateau. *Remote Sens.* **2014**, *6*, 8337–8358. [[CrossRef](#)]

35. Na, L.; Zhang, J.; Bao, Y.; Bao, Y.; Na, R.; Tong, S.; Si, A. Himawari-8 satellite based dynamic monitoring of grassland fire in China-Mongolia border regions. *Sensors* **2018**, *18*, 276. [[CrossRef](#)]
36. Liu, X.; Zhang, J.; Tong, Z.; Bao, Y. Gis-based multi-dimensional risk assessment of the grassland fire in northern China. *Nat. Hazards* **2012**, *64*, 381–395. [[CrossRef](#)]
37. Bao, Y.L.; Zhang, J.Q.; Liu, X.P.; Chen, P.; Liu, X.J.; Zhang, Q. Analysis on grass fire traces extracted and pre-disaster characteristics of combustibles based on hj-1b satellite data. *J. Catastrophology* **2013**, *28*, 32–45.
38. Zhang, J.; Cui, L.; Tong, Z.; Liu, X.; Bao, Y. Grid gis and optimal segmentation based early warning of grassland fire disaster risk threshold in Hulunbeier grassland. *Syst. Eng.-Theory Pract.* **2013**, *33*, 770–775.
39. Liu, M.; Yang, L. Human-caused fires release more carbon than lightning-caused fires in the conterminous United States. *Environ. Res. Lett.* **2020**, *16*, 014013. [[CrossRef](#)]
40. Chen, G.; Hayes, D.J.; David McGuire, A. Contributions of wildland fire to terrestrial ecosystem carbon dynamics in North America from 1990 to 2012. *Glob. Biogeochem. Cycles* **2017**, *31*, 878–900. [[CrossRef](#)]
41. Na, R.; Na, L.; Du, H.; He, H.S.; Shan, Y.; Zong, S.; Huang, L.; Yang, Y.; Wu, Z. Vegetation greenness variations and response to climate change in the arid and semi-arid transition zone of the Mongolian plateau during 1982–2015. *Remote Sens.* **2021**, *13*, 4066. [[CrossRef](#)]
42. Luo, M.; Meng, F.; Sa, C.; Duan, Y.; Bao, Y.; Liu, T.; De Maeyer, P. Response of vegetation phenology to soil moisture dynamics in the Mongolian plateau. *Catena* **2021**, *129*, 107945. [[CrossRef](#)]
43. Neupert, R.F. Population, nomadic pastoralism and the environment in the Mongolian plateau. *Popul. Environ.* **1999**, *20*, 413–441. [[CrossRef](#)]
44. Feng, Z.D.; Zhai, X.W.; Ma, Y.Z.; Huang, C.Q.; Wang, W.G.; Zhang, H.C.; Khosbayar, P.; Narantsetseg, T.; Liu, K.B.; Rutter, N.W. Eolian environmental changes in the northern Mongolian plateau during the past~35,000 year. *Palaeogeogr. Palaeoclimatol. Palaeoecol.* **2007**, *245*, 505–517. [[CrossRef](#)]
45. Liu, J.; Qi, Y.; Shi, H.; Zhuang, D.; Hu, Y. Estimation of wind erosion rates by using <sup>137</sup>cs tracing technique: A case study in Tariat-Xilin Gol Transect, Mongolian plateau. *Chin. Sci. Bull.* **2008**, *53*, 751–758. [[CrossRef](#)]
46. Zhang, X.; Hu, Y.; Zhuang, D.; Qi, Y.; Ma, X. Ndvi spatial pattern and its differentiation on the Mongolian plateau. *J. Geogr. Sci.* **2009**, *19*, 403–415. [[CrossRef](#)]
47. Bao, G.; Bao, Y.; Qin, Z.; Xin, X.; Bao, Y.; Bayarsaikhan, S.; Zhou, Y.; Chuntai, B. Modeling net primary productivity of terrestrial ecosystems in the semi-arid climate of the Mongolian plateau using lswi-based casa ecosystem model. *Int. J. Appl. Earth Obs. Geoinf.* **2016**, *46*, 84–93. [[CrossRef](#)]
48. Bao, G.; Jin, H.; Tong, S.; Chen, J.; Huang, X.; Bao, Y.; Shao, C.; Mandakh, U.; Chopping, M.; Du, L. Autumn phenology and its covariation with climate, spring phenology and annual peak growth on the Mongolian plateau. *Agric. For. Meteorol.* **2021**, *298–299*, 108312. [[CrossRef](#)]
49. Zhao, X.; Shen, H.; Geng, X.; Fang, J. Three-decadal destabilization of vegetation activity on the Mongolian plateau. *Environ. Res. Lett.* **2021**, *16*, 034049. [[CrossRef](#)]
50. Bao, G.; Chen, J.; Chopping, M.; Bao, Y.; Bayarsaikhan, S.; Dorjsuren, A.; Tuya, A.; Jirigala, B.; Qin, Z. Dynamics of net primary productivity on the Mongolian plateau: Joint regulations of phenology and drought. *Int. J. Appl. Earth Obs. Geoinf.* **2019**, *81*, 85–97. [[CrossRef](#)]
51. Chen, J.; John, R.; Sun, G.; Fan, P.; Henebry, G.M.; Fernández-Giménez, M.E.; Zhang, Y.; Park, H.; Tian, L.; Groisman, P.; et al. Prospects for the sustainability of social-ecological systems (ses) on the Mongolian plateau: Five critical issues. *Environ. Res. Lett.* **2018**, *13*, 123004. [[CrossRef](#)]
52. Hilker, T.; Natsagdorj, E.; Waring, R.H.; Lyapustin, A.; Wang, Y. Satellite observed widespread decline in Mongolian grasslands largely due to overgrazing. *Glob. Change Biol.* **2014**, *20*, 418–428. [[CrossRef](#)]
53. Gunin, P.D.; Saandar, M. *Ecosystems of Mongolia: Atlas*; Institute of Ecology and Evolution, Russian Academy of Sciences: Moscow, Russia, 2019.
54. Xu, D.; Ding, W. *Impacts and Risks of Climate Change: Impacts and Risks of Climate Change on Desertification*; Science Press: Beijing, China, 2016.
55. Ord, J.K.; Getis, A. Local spatial autocorrelation statistics distributional issues and an application. *Geograph. Anal.* **1995**, *27*, 286–306. [[CrossRef](#)]
56. Mann, B.H.B. Nonparametric tests against trend. *J. Econom. Soc.* **1945**, *13*, 245–259. [[CrossRef](#)]
57. Fan, P.Y.; Chun, K.P.; Mijic, A.; Tan, M.L.; He, Q.; Yetemen, O. Quantifying land use heterogeneity on drought conditions for mitigation strategies development in the Dongjiang river basin, China. *Ecol. Indic.* **2021**, *129*, 107945. [[CrossRef](#)]
58. Sun, J.Y.; Li, M.Z.; Zheng, L.H.; Hu, Y.G.; Zhang, X.J. Real-time analysis of soil moisture, soil organic matter, and soil total nitrogen with nir spectra. *Spectrosc. Spectr. Anal.* **2006**, *26*, 426–429.
59. Na, R.; Du, H.; Na, L.; Shan, Y.; He, H.S.; Wu, Z.; Zong, S.; Yang, Y.; Huang, L. Spatiotemporal changes in the aeolian desertification of Hulunbuir grassland and its driving factors in China during 1980–2015. *Catena* **2019**, *182*, 10412. [[CrossRef](#)]
60. Yue, J.; Tian, Q. Estimating fractional cover of crop, crop residue, and soil in cropland using broadband remote sensing data and machine learning. *Int. J. Appl. Earth Obs. Geoinf.* **2020**, *89*, 1–15. [[CrossRef](#)]

61. Li, Y.; Zhao, J.; Guo, X.; Zhang, Z.; Tan, G.; Yang, J. The influence of land use on the grassland fire occurrence in the northeastern Inner Mongolia autonomous region, China. *Sensors* **2017**, *17*, 437. [[CrossRef](#)]
62. Wu, L.; Ma, X.; Dou, X.; Zhu, J.; Zhao, C. Impacts of climate change on vegetation phenology and net primary productivity in arid Central Asia. *Sci. Total Environ.* **2021**, *796*, 149055. [[CrossRef](#)]
63. Sharma, S.; Carlson, J.D.; Krueger, E.S.; Engle, D.M.; Twidwell, D.; Fuhlendorf, S.D.; Patrignani, A.; Feng, L.; Ochsner, T.E. Soil moisture as an indicator of growing-season herbaceous fuel moisture and curing rate in grasslands. *Int. J. Wildland Fire* **2021**, *30*, 57–69. [[CrossRef](#)]
64. Sukhbaatar, G.; Purevragchaa, B.; Ganbaatar, B.; Tseveen, B. Deforestation and degradation of forests in the Khustai Nuruu mountains of Northern Mongolia. *Sib. J. For. Sci.* **2021**, *62*, 53–63.
65. Che, M.; Chen, B.; Innes, J.L.; Wang, G.; Dou, X.; Zhou, T.; Zhang, H.; Yan, J.; Xu, G.; Zhao, H. Spatial and temporal variations in the end date of the vegetation growing season throughout the Qinghai–Tibetan plateau from 1982 to 2011. *Agric. For. Meteorol.* **2014**, *189–190*, 81–90. [[CrossRef](#)]
66. Bai, Y.; Zha, T.; Bourque, C.P.-A.; Jia, X.; Ma, J.; Liu, P.; Yang, R.; Li, C.; Du, T.; Wu, Y. Variation in ecosystem water use efficiency along a Southwest-to-Northeast aridity gradient in China. *Ecol. Indic.* **2020**, *110*, 105932. [[CrossRef](#)]
67. Yuan, H.Y. Analysis of Spatial-Temporal Changes of Vegetation Ndvi in Border Areas of China-Mongolia. Master's Thesis, College of Geographical Science, Inner Mongolia Normal University, Hohhot, China, 2016.
68. Sukhbaatar, B.; Ulziikhutag, O.; Sukhbaatar, T. A Study on e-Government Policy in Mongolia. In Proceedings of the Symposium on Information & Telecommunication Technologies, Bangkok, Thailand, 20 September–18 October 2006.
69. Olji; Bolor; Gerelchoktu; Liu, S. Present situation and protection in Daurian steppe ecological area. *J. MUC Nat. Sci. Ed.* **2013**, *12*, 24–26.
70. Wang, G.; Wang, J.; Zou, X.; Chai, G.; Wu, M.; Wang, Z. Estimating the fractional cover of photosynthetic vegetation, non-photosynthetic vegetation and bare soil from modis data: Assessing the applicability of the ndvi-dfi model in the typical Xilingol grasslands. *Int. J. Appl. Earth Obs. Geoinf.* **2019**, *76*, 154–166. [[CrossRef](#)]
71. Guo, Z.; Kurban, A.; Ablekim, A.; Wu, S.; Van de Voorde, T.; Azadi, H.; Maeyer, P.D.; Dufatanye Umwali, E. Estimation of photosynthetic and non-photosynthetic vegetation coverage in the lower reaches of Tarim river based on sentinel-2a data. *Remote Sens.* **2021**, *13*, 1458. [[CrossRef](#)]
72. Zhou, R.; Yang, G.; Ping, M. Exploitation and utilization of natural grassland in Greater Khingan mountains. *Nat. Resour. Res.* **1987**, *4*, 44–50.
73. Gao, J.; Zhao, Y.; Xu, W.; Chen, X.; Bao, Y. Exploitation and utilization of interforest margin grassland in Greater Khingan mountains. *Inn. Mong. For. Sci. T Echnology* **2001**, 84–85.
74. Cao, X.; Chen, J.; Matsushita, B.; Imura, H. Developing a modis-based index to discriminate dead fuel from photosynthetic vegetation and soil background in the Asian steppe area. *Int. J. Remote Sens.* **2010**, *31*, 1589–1604. [[CrossRef](#)]
75. Liu, X.; Zhang, J.; Tong, Z. Modeling the early warning of grassland fire risk based on fuzzy logic in Xilingol, Inner Mongolia. *Nat. Hazards* **2014**, *75*, 2331–2342. [[CrossRef](#)]
76. Chai, G.; Wang, J.; Wu, M.; Li, G.; Zhang, L.; Wang, Z. Mapping the fractional cover of non-photosynthetic vegetation and its spatiotemporal variations in the Xilingol grassland using modis imagery (2000–2019). *Geocarto Int.* **2020**, *37*, 1863–1879. [[CrossRef](#)]
77. Atchley, A.L.; Linn, R.; Jonko, A.; Hoffman, C.; Hyman, J.D.; Pimont, F.; Sieg, C.; Middleton, R.S. Effects of fuel spatial distribution on wildland fire behaviour. *Int. J. Wildland Fire* **2021**, *30*, 179. [[CrossRef](#)]
78. Jin, Y.X.; Xu, B.; Yang, X.C.; Li, J.Y.; Wang, D.L.; Ma, H.L. Remote sensing dynamic estimation of grass production in Xilinguole, Inner Mongolia. *Sci. Sin. Vitae* **2011**, *41*, 1185–1195.
79. Gu, Z.J.; Zeng, Z.Y. Overview of researches on vegetation coverage in remote sensing. *Res. Soil Water Conserv.* **2005**, *12*, 18–21.
80. Hernandez-Leal, P.A.; Arbelo, M.; Gonzalez-Calvo, A. Fire risk assessment using satellite data. *Adv. Space Res.* **2006**, *37*, 741–746. [[CrossRef](#)]
81. Savage, M.; Swetnam, T.W. Early 19th-century fire decline following sheep pasturing in a Navajo Ponderosa pine forest. *Ecology* **1990**, *71*, 2374–2378. [[CrossRef](#)]
82. Zhang, X.; Xiao, X.; Qiu, S.; Xu, X.; Wang, X.; Chang, Q.; Wu, J.; Li, B. Quantifying latitudinal variation in land surface phenology of spartina alterniflora saltmarshes across coastal wetlands in China by landsat 7/8 and sentinel-2 images. *Remote Sens. Environ.* **2022**, *269*, 112810. [[CrossRef](#)]
83. Zhu, W.; Tian, H.; Xu, X.; Pan, Y.; Chen, G.; Lin, W. Extension of the growing season due to delayed autumn over mid and high latitudes in North America during 1982–2006. *Glob. Ecol. Biogeogr.* **2012**, *21*, 260–271. [[CrossRef](#)]
84. Shen, M.; Jiang, N.; Peng, D.; Rao, Y.; Huang, Y.; Fu, Y.H.; Yang, W.; Zhu, X.; Cao, R.; Chen, X. Can changes in autumn phenology facilitate earlier green-up date of northern vegetation? *Agric. For. Meteorol.* **2020**, *291*, 108077. [[CrossRef](#)]
85. Battulga, P.; Tsogtbaatar, J.; Dulamsuren, C.; Hauck, M. Equations for estimating the above-ground biomass of larch sibirica in the forest-steppe of Mongolia. *J. For. Res.* **2013**, *24*, 431–437. [[CrossRef](#)]

86. Usoltsev, V.A.; Danilin, I.M.; Zaandrabalyn Tsogt, Z.; Anna, A.; Osmirko, A.A.; Tsepordey, I.S.; Chasovskikh, V.P. Aboveground biomass of Mongolian larch (*Larix sibirica* ledeb.) forests in the Eurasian region. *Geogr. Environ. Sustain.* **2019**, *12*, 117–132. [[CrossRef](#)]
87. Zeng, W.S.; Duo, H.R.; Lei, X.D.; Chen, X.Y.; Wang, X.J.; Pu, Y.; Zou, W.T. Individual tree biomass equations and growth models sensitive to climate variables for *larix* spp. in China. *Eur. J. For. Res.* **2017**, *136*, 233–249. [[CrossRef](#)]

**Disclaimer/Publisher’s Note:** The statements, opinions and data contained in all publications are solely those of the individual author(s) and contributor(s) and not of MDPI and/or the editor(s). MDPI and/or the editor(s) disclaim responsibility for any injury to people or property resulting from any ideas, methods, instructions or products referred to in the content.